

1 **Zika virus infection preferentially counterbalances human peripheral**  
2 **monocyte and/or NK-cell activity**

3

4 Fok-Moon Lum<sup>1</sup>, David Lee<sup>2</sup>, Tze-Kwang Chua<sup>1</sup>, Jeslin J.L. Tan<sup>1</sup>, Cheryl Y.P.  
5 Lee<sup>1,3</sup>, Xuan Liu<sup>4,5</sup>, Yongxiang Fang<sup>4</sup>, Bennett Lee<sup>1</sup>, Wearn-Xin Yee<sup>1</sup>, Natasha  
6 Y. Rickett<sup>5,6</sup>, Po-Ying Chia<sup>7</sup>, Vanessa Lim<sup>7</sup>, Yee-Sin Leo<sup>7,8,9</sup>, David A.  
7 Matthews<sup>2</sup>, Julian A. Hiscox<sup>1,5,6\*</sup>, Lisa F.P. Ng<sup>1,5,6,10\*</sup>

8

9 <sup>1</sup>Singapore Immunology Network, Agency for Science, Technology and  
10 Research (A\*STAR), Singapore 138648, Singapore.

11 <sup>2</sup>School of Cellular and Molecular Medicine, University of Bristol, Bristol BS8  
12 1TD, UK.

13 <sup>3</sup>NUS Graduate School for Integrative Sciences and Engineering, National  
14 University of Singapore, Singapore 117456, Singapore.

15 <sup>4</sup>Centre for Genomic Research, Institute of Integrative Biology, University of  
16 Liverpool, Liverpool L69 7ZB, UK.

17 <sup>5</sup>National Institute of Health Research, Health Protection Research Unit In  
18 Emerging and Zoonotic Infections, University of Liverpool, Liverpool L69 3GL,  
19 UK.

20 <sup>6</sup>Institute of Infection and Global Health, University of Liverpool, Liverpool L69  
21 7BE, UK.

22 <sup>7</sup>Communicable Diseases Centre, Institute of Infectious Diseases and  
23 Epidemiology, Tan Tock Seng Hospital, Singapore 308433, Singapore.

24 <sup>8</sup>Lee Kong Chian School of Medicine, Nanyang Technological University,  
25 Singapore 636921, Singapore.

26 <sup>9</sup>Saw Swee Hock School of Public Health, National University of Singapore,  
27 Singapore 117549, Singapore.

28 <sup>10</sup>Department of Biochemistry, Yong Loo Lin School of Medicine, National  
29 University of Singapore, Singapore 117597, Singapore.

30

31 Correspondence: Prof Lisa F.P. Ng ([lisa\\_ng@immunol.a-star.edu.sg](mailto:lisa_ng@immunol.a-star.edu.sg)); Prof

32 Julian A. Hiscox ([Julian.Hiscox@liverpool.ac.uk](mailto:Julian.Hiscox@liverpool.ac.uk))

33

34 Abstract: 172 words

35 Main text: 9035 words

36 Inserts: 8 Figures and 2 Tables

37 **Abstract**

38 Zika virus (ZIKV) has re-emerged in the population and caused  
39 unprecedented global outbreaks. Here, the transcriptomic consequences of  
40 ZIKV infection were studied systematically firstly in human peripheral blood  
41 CD14<sup>+</sup> monocytes and monocyte-derived macrophages with high density  
42 RNA-sequencing. Analyses of the ZIKV genome revealed that the virus  
43 underwent genetic diversification and differential mRNA abundance was  
44 found in host cells during infection. Notably, there was a significant change in  
45 the cellular response with crosstalk between monocytes and natural killer  
46 (NK) cells as one of the highly identified pathway. Immune-phenotyping of  
47 peripheral blood from ZIKV-infected patients further confirmed the activation  
48 of NK cells during acute infection. ZIKV infection in peripheral blood cells  
49 isolated from healthy donors led to the induction of IFN $\gamma$  and CD107a — two  
50 key markers of NK-cell function. Depletion of CD14<sup>+</sup> monocytes from  
51 peripheral blood resulted in a reduction of these markers and reduced priming  
52 of NK cells during infection. This was complemented by the immunoproteomic  
53 changes observed. Mechanistically, ZIKV infection preferentially  
54 counterbalances monocyte and/or NK-cell activity, with implications for  
55 targeted cytokine immunotherapies.

56 **Importance**

57 Zika virus (ZIKV), an infectious agent, which has re-emerged over the recent  
58 years, has been associated with causing congenital brain deformities. While  
59 numerous studies have focused on understanding the mechanisms of ZIKV  
60 pathogenesis, little knowledge is available for describing host cell immune  
61 response during active infection. ZIKV is transmitted via the bites of infected  
62 female *Aedes* mosquitoes and subsequently travels to the blood stream  
63 where it will encounter the peripheral immune cells. Recent studies have  
64 shown that the blood monocytes are targets of ZIKV, and thus understanding  
65 the response of these cells during infection would be critical as virus-host  
66 interaction determines disease progression. The significance of this study  
67 highlights the important immune pathways elicited by the monocytes during  
68 infection and further provides a model for the functional study of these cells  
69 and their fellow immune partners, with implications for the development of  
70 future immune-based therapies.

## 71 **Introduction**

72 Zika virus (ZIKV) gained global attention in 2015-2016 when the virus  
73 suddenly re-emerged in the human population and caused major viral  
74 outbreaks across the world with a large disease burden (1). Although ZIKV  
75 has been causing sporadic outbreaks since it was first reported in Uganda  
76 >60 years ago (2), very little is known about the biology of the virus and the  
77 host response to infection. ZIKV is an arthropod-borne flavivirus that causes  
78 Zika fever — a disease that for the majority of patients has little or no  
79 symptoms (3). However, in severe cases, ZIKV infection may be  
80 responsible for neurological complications such as Guillain Barré Syndrome  
81 (GBS) in adults (4) and congenital fetal growth-associated anomalies in  
82 newborns (5). The host response to ZIKV infection may be one of the main  
83 drivers of the different disease phenotypes.

84         Recent studies have established that ZIKV can infect peripheral  
85 blood monocytes (6-9). However, despite ongoing intensive investigative  
86 efforts to understand ZIKV-related neuropathogenesis, knowledge  
87 regarding the mechanisms of ZIKV infection in peripheral immune cells is  
88 lacking. Given that ZIKV is transmitted into the dermis via the bite from a  
89 virus-infected mosquito, monocytes would be one of the first immune cells  
90 in the blood to interact with the virus when it reaches the circulatory system.  
91 Therefore, the interplay between ZIKV and monocytes will be crucial in  
92 determining the outcome of infection (10).

93         This study focused on characterising the primary *ex vivo* response of  
94 human donor blood monocytes and monocyte-derived macrophages  
95 (MDMs) to ZIKV infection. Systematically, RNA-sequencing (RNA-seq) was

96 first used to identify and quantify the abundance of host messenger RNA  
97 (mRNA) and characterise viral RNA. This information was subsequently  
98 used to map the host response to ZIKV infection in the two different *ex vivo*  
99 cell types. These data also provided insights into the potential adaptation of  
100 the virus during viral replication in these cells. Immune-phenotyping of  
101 peripheral blood cells isolated from patients infected with ZIKV  
102 independently was executed to validate the predictions obtained from the  
103 differential gene expression analysis. Depletion of CD14<sup>+</sup> monocytes in  
104 peripheral blood was then performed *ex vivo* to functionally understand the  
105 crosstalk between monocytes and priming of NK cells during ZIKV infection.  
106 Lastly, a multiplex assay was carried out to further understand host cell  
107 immunoproteomic changes during ZIKV infection. To our knowledge, this  
108 study is the first large-scale systematic investigation into the host cellular  
109 response to ZIKV infection in biologically relevant cells. This global analysis  
110 of the host immune response provides a novel understanding of the  
111 pathobiology of the virus, leading to the possibility of targeted therapeutic  
112 interventions in severe cases.

113 **Results**

114 **ZIKV targets human peripheral blood monocytes and macrophages.**

115 CD14<sup>+</sup> monocytes have been reported to be the main targets of ZIKV  
116 during infection (6-9). In this study, human primary CD14<sup>+</sup> monocytes were  
117 first isolated from fresh peripheral blood mononuclear cells (PBMCs) to  
118 enrich this cell type to >90% of the total cell population (Figure 1A). In  
119 addition, isolated monocytes from the same donors were differentiated into  
120 monocytes-derived macrophages (MDMs) over 5 days (Figure 1B). Purified  
121 cells were then infected *ex vivo* with ZIKV and their permissiveness to ZIKV  
122 infection and growth was determined at 24 and 72 hours post-infection (hpi)  
123 (Figure 1A). The early time point was chosen to cover the acute infection  
124 phase and the later time point a stage by which a substantial host-virus  
125 interaction would have taken place (11). Data obtained showed that ZIKV  
126 infection of MDMs was greater than infection of monocytes in all five donors  
127 (~40% compared to ~20% at 72 hpi, respectively) (Figure 1C). A decrease  
128 in viral load was observed in the virus-infected MDMs between the two time  
129 points, whereas the viral load remained consistent in infected monocytes  
130 over time (Figure 1D).

131 To further show that monocytes are the main targets of ZIKV  
132 infection, PBMCs obtained from four healthy human volunteers were  
133 infected and the percentage of ZIKV antigen positive cells was determined  
134 in the different immune subsets (Supplemental Figure 1A and 1B). ZIKV  
135 antigen was detected in the CD14<sup>+</sup> monocytes (~6%), while infection of T,  
136 natural killer (NK), NKT, and B cells by ZIKV was negligible (Supplemental  
137 Figure 1B and 1C). These data suggested that these cell types were either

138 refractive or infected at levels below the detection limits at the chosen time-  
139 points. The overall viral load in ZIKV-infected PBMCs was not significantly  
140 different between 24 and 72 hpi (Supplemental Figure 1D).

141

142 **Genome variation in ZIKV during infection of the peripheral blood.** In  
143 order to compare the amount of virus between the different cell types and  
144 determine whether ZIKV underwent genetic diversification during infection,  
145 viral sequence reads were mapped and compared to that of the progenitor  
146 virus stock (PF/ZIKV/HPF/2013). These data indicated that for MDMs, 4.53%  
147 and 0.43% of total sequence reads mapped to the ZIKV genome at 24 hpi and  
148 72 hpi, respectively. While 24% and 0.8% of sequence reads generated from  
149 monocytes mapped to the ZIKV genome at 24 hpi and 72 hpi respectively.  
150 These observations are consistent with ZIKV viral load analysis, where higher  
151 levels of viral RNA were detected in MDMs (Figure 1).

152         Due to the inherent error-prone nature of viral RNA replication,  
153 nucleotide variants may become established in the viral genome during ZIKV  
154 infection in different cell types. To investigate this hypothesis, consensus  
155 genome information for each sample and the frequency of minor variants at  
156 each nucleotide position in the progenitor stock was determined and  
157 compared to the genome of virus present in the infected samples utilizing  
158 previously developed workflows (12,13). The ZIKV consensus genome  
159 sequence derived from the progenitor stock was 10,570 nucleotides in length  
160 and contained minor variants (as a measure of quasi-species) spread  
161 throughout the genome (Figure 2A). Of the 11 valid consensus sequences  
162 derived from the virus-infected samples, the virus recovered in cells from five



163 donors (D1-D5) had the same consensus sequence as the input stock  
164 (PF/ZIKV/HPF/2013). However, some donor samples contained viral  
165 genomes that had additional nucleotide differences at six different positions  
166 (Table 1). These nucleotide differences (Table 1) were visualized as a  
167 maximum likelihood phylogenetic tree, where the input stock was used as the  
168 reference sample (Figure 2B). There were only eight high frequency transition  
169 mutations to choose from ( $\log_{10}8 = 0.9$ , see Figure 2A), increasing the  
170 likelihood of these changes appearing several times. Of these eight transition  
171 mutations, six appeared as major variants and thus changed the overall  
172 consensus sequence. The nucleotide positions of these six transition  
173 mutations (Table 2) indicated that all the changes in the consensus sequence  
174 were already present at relatively high frequency as minor variants in the input  
175 stock and were subsequently amplified during viral replication. Changes at  
176 nucleotide positions 2,815 and 4,211 were the most common, being found in  
177 ~35% reads mapping to the virus genome. Had these changes been found in  
178  $\geq 50\%$  reads, they would have been classified as major variants and thus  
179 changed the consensus sequence (Table 2).

180

181 **Transcriptomic profiling reveals key cellular responses to ZIKV**  
182 **infection.** RNA-seq was used to identify and quantify global mRNA  
183 abundance in ZIKV-infected peripheral monocytes and MDMs at 24 and 72  
184 hpi. mRNA purified from 27 samples showed no signs of degradation and had  
185 sufficient read depth for inclusion in the analyses (Supplemental Figure 2A).  
186 For monocytes, mock and ZIKV-infected cells at both 24 and 72 hpi exhibited  
187 minimal changes in host transcript abundance. For MDMs, the abundance of

188 transcripts that mapped to 1,736 and 545 genes at 24 and 72 hpi respectively,  
189 were significantly different (FDR < 0.05) between the mock and ZIKV-infected  
190 samples (Supplemental Figure 2B).

191 Ingenuity Pathway Analysis (IPA) was used to interrogate and group  
192 the differentially expressed genes into functional pathways (Figure 3A). A total  
193 of 169 pathways were identified, of which 27 were common in ZIKV-infected  
194 MDMs at 24 and 72 hpi. A further 106 pathways were unique to samples at 24  
195 hpi (Supplemental Table S1), and 36 pathways were unique to samples at 72  
196 hpi (Supplemental Table S2). This analysis found that genes associated with  
197 the interferon response were significantly upregulated at both time-points. In  
198 addition, signalling pathways involved in the pathogenesis of multiple  
199 sclerosis, and key pathways involved in monocyte-derived dendritic cell  
200 (moDCs) and NK cell processes were also shared between the two time  
201 points (Figure 3A). Overall, the top three common pathways activated in  
202 MDMs were interferon signalling, multiple sclerosis pathogenic pathways and  
203 crosstalk pathways between moDCs and NK cells (Figure 3A). The specific  
204 genes with the most abundant transcripts within these three pathways were  
205 analyzed, and when compared to the mock-infected controls were all  
206 increased in abundance after ZIKV infection (Figure 3B).

207

### 208 **Virus-infected MDMs exhibit reduced cellular responsiveness.**

209 Transcriptomic profiles of various ZIKV-infected MDMs were compared to  
210 evaluate the transition of the cellular host response over the course of ZIKV  
211 infection. The percentage overlap of the identified transcripts between ZIKV-  
212 infected MDMs was assessed at 24 hpi and 72 hpi within the three targeted

213 pathways described above (Figure 4). Interestingly, the percentage of  
214 overlapping transcripts identified at 72 hpi was lower for all three pathways,  
215 which may reveal a lower activation status of these pathways at this stage of  
216 the infection. The identification of different transcripts associated with 72 hpi  
217 may indicate the different signalling cascades present or activation status of  
218 these cells (Figure 4A). Global assessment of all identified transcripts  
219 revealed that transcripts mapping to 251 genes were in fact present in virus-  
220 infected MDMs at both time points. Transcripts that mapped to 1,485 genes  
221 were specific to 24 hpi, of which 54.81% exhibited greater abundance  
222 compared to the mock controls. By comparison, transcripts that mapped to  
223 294 genes were unique to 72 hpi, with 63.36% of them having greater mRNA  
224 abundance compared to the mock controls (Figure 4B). Within the 251  
225 common genes, transcripts mapping to 218 genes had a greater fold-change  
226 value compared to the mock-infected controls, indicating that these transcripts  
227 were increased in abundance in all ZIKV-infected MDMs. Further inquiry of  
228 these transcripts revealed that 60.1% of them were greater in abundance at  
229 72 hpi compared to 24 hpi. Likewise, of the remaining transcripts that mapped  
230 to 33 genes and showed decreased abundance, 84.85% were further reduced  
231 at 72 hpi.

232

233 **NK cells are activated in ZIKV-infected patients.** IPA predicted robust  
234 crosstalk between NK cells and moDCs in peripheral blood upon *ex vivo*  
235 ZIKV infection (Figure 3-4). The IPA prediction that NK cells were activated  
236 in the peripheral blood of ZIKV-infected patients was, therefore,  
237 investigated by comprehensive immune-phenotyping of blood samples

238 taken from ZIKV-infected patients. These patients were recruited from the  
239 first endemic ZIKV outbreak in Singapore in 2016 (7,14). Blood aliquots  
240 were obtained from ZIKV-infected patients (n=9) during the acute disease  
241 phase (between 1 and 7 days post-illness-onset), and were subjected to a  
242 whole blood staining protocol that targeted CD56<sup>+</sup> cells, predominantly NK  
243 cells (15) (Figure 5A). Blood from healthy donors (n=5) was collected and  
244 processed in parallel as a control group. Gated cells were further grouped  
245 with the C-type lectin receptor CD94, giving three CD56<sup>+</sup> populations:  
246 CD56<sup>bright</sup>CD94<sup>hi</sup>, CD56<sup>dim</sup>CD94<sup>hi</sup> and CD56<sup>dim</sup>CD94<sup>lo</sup> (16). The activation  
247 status of these populations was then assessed based on the percentage of  
248 each subset expressing CD16 and CD69 (Figure 5B). A higher level of  
249 CD16 was observed across all CD56<sup>+</sup> subsets in ZIKV-infected patients  
250 compared to the healthy controls. A higher percentage of the subsets also  
251 expressed CD69 — a known cellular activation marker (17).

252

253 **CD14<sup>+</sup> monocytes prime NK-cell activity during ZIKV infection.** Given that  
254 peripheral NK cells were activated in ZIKV-infected patients and that the  
255 precursor of MDMs was the monocytes, the functional relationship between  
256 monocytes and NK cells were assessed. This relationship is critical especially  
257 during the viremic phase. Briefly, CD14<sup>+</sup> monocytes were depleted from  
258 human primary PBMCs, with an average efficiency of >95% (Supplemental  
259 Figure 3). Lipopolysaccharide (LPS; 10ng/ml) was used as a positive control  
260 to stimulate monocytes to prime NK cells (18). A significant reduction in the  
261 activity of NK cells was observed when CD14-depleted PBMCs were  
262 stimulated with LPS compared to LPS stimulation of PBMCs containing

263 CD14<sup>+</sup> monocytes (Supplemental Figure 4). This effect was evidenced by the  
264 reduced levels of the surface markers CD69, CD107a and intracellular IFN $\gamma$  in  
265 depleted cells, verifying that this approach was an efficient strategy for  
266 investigating the relationship between monocytes and NK cells.

267 PBMCs were then isolated from seven healthy donors and subjected to  
268 CD14-depletion before being either infected with ZIKV or stimulated with LPS  
269 in parallel to serve as a control to determine activation of NK cells. ZIKV  
270 infection in non-depleted PBMCs resulted in high levels of CD107a and IFN $\gamma$   
271 (Figure 6A) in CD56<sup>+</sup>CD94<sup>+</sup> NK cells (Supplemental Figure 5) at 36 hpi — an  
272 optimal time-point to detect NK-cell priming (19). The opposite effect,  
273 however, was observed in ZIKV-infected PBMCs depleted of CD14<sup>+</sup>  
274 monocytes as the levels of both CD107a and IFN $\gamma$  were significantly reduced  
275 (Figure 6B). The levels of CD107a and IFN $\gamma$  remained high at 72 hpi in non-  
276 depleted infected PBMCs compared to depleted infected PBMCs  
277 (Supplemental Figure 6). Interestingly, although monocyte depletion did not  
278 affect the expression of NK-cell activation receptors NKG2A or NKG2D, a  
279 general reduction in NKG2D-expressing NK cells was observed during ZIKV  
280 infection (Supplemental Figure 7A and 7B). Surprisingly, the activation marker  
281 CD69 was not increased upon ZIKV infection in this study (Supplemental  
282 Figure 7C and 7D). ZIKV viral load was comparable between both conditions  
283 (Figure 6C).

284 To delve further into the mechanism, the profile of secreted immune  
285 mediators from ZIKV-infected PBMCs was quantified using a 45-plex  
286 microbead-based immunoassay (20). Levels of 11 mediators were  
287 significantly affected by the depletion of CD14<sup>+</sup> monocytes (Figure 7A and

288 Supplemental Figure 8A), while 8 mediators were affected upon ZIKV  
289 infection (Supplemental Figure 8B). Interestingly, depletion of CD14<sup>+</sup>  
290 monocytes and ZIKV infection did not affect the levels of EGF, IL-9, IL-17A,  
291 MIP-1 $\alpha$  and MIP-1 $\beta$  (Supplemental Figure 8C). The effect of CD14<sup>+</sup>  
292 monocytes depletion was observed in the levels of SCF and TNF $\alpha$  only after  
293 ZIKV infection (Supplemental Figure 8D). Importantly, levels of MCP-1, IL1RA  
294 and VEGF-A were affected by both CD14<sup>+</sup> monocytes depletion and ZIKV  
295 infection (Figure 7B). To further investigate the capacity of the cytokine  
296 milieu in priming NK cells, freshly isolated human primary PBMCs were then  
297 treated with the same culture supernatants from ZIKV-infected PBMCs and  
298 CD14<sup>+</sup> monocytes-depleted PBMCs. Stimulation with culture supernatant from  
299 ZIKV-infected non-depleted PBMCs led to slightly more cell death  
300 (Supplemental Figure 9A) accompanied by a significant upregulation in  
301 expression of CD107a, IFN $\gamma$  and NKG2D in the CD94<sup>+</sup>CD56<sup>+</sup> NK cells (Figure  
302 7C and Supplemental Figure 9B), confirming the importance of monocytes in  
303 NK-cell priming during ZIKV infection. To rule out priming of NK cells by  
304 viruses present in the culture supernatant, a UV-treatment procedure was  
305 performed to inactivate the virus, prior to the stimulation assay. Expectedly,  
306 while UV-inactivation successfully inactivated ZIKV (Supplemental Figure  
307 10A), it also affected the quality of the cytokines and led to reduced priming of  
308 NK cells (Supplemental Figure 10B).

309 **Discussion**

310 Myeloid cells are targets of active ZIKV infection (6-9,21-23) and can elicit  
311 immune responses with detrimental outcomes (6,8). Both monocytes and  
312 macrophages exhibit extensive heterogeneity (24,25). While it is difficult to  
313 obtain tissue-resident macrophages for experimental purposes, human  
314 blood is a readily accessible, valuable source of these cells. Transcriptomic  
315 profiling of *ex vivo* human blood monocytes and MDMs has revealed  
316 marked differences between these cell types (26,27). In this study, human  
317 primary monocytes were naturally differentiated into MDMs without any bias  
318 for an M1 or M2 macrophage phenotype (28). Given that these cells are  
319 targets of ZIKV infection (8), investigations into their cellular immune  
320 responses during infection will open avenues to exploit their function for  
321 therapeutic benefits.

322         The level of ZIKV infection (as assessed by the amount of ZIKV  
323 antigen and genome copy number) was higher in MDMs than monocytes,  
324 which corroborates previous observations (8). Transcriptomic differences  
325 between monocytes and MDMs (26,27) would be a plausible explanation  
326 for the differential susceptibility of these cells to ZIKV infection. It is also  
327 noteworthy that higher ZIKV infection levels were found in purified primary  
328 cell populations compared to PBMCs, perhaps due to the presence of other  
329 immune subsets in PBMCs that may dampen the overall infection level.  
330 ZIKV RNA was detected at the two time-points, 24 and 72 hpi and the virus  
331 was present as quasi-species post-infection in human primary myeloid  
332 cells. The virus consensus sequence and minor variant mapping revealed  
333 an over-representation of transition mutations at highly variable nucleotide

334 positions in the sequence reads. The proportion of these minor variants  
335 indicated a shift towards becoming major variants. A recent study that  
336 sequenced ZIKV genomes isolated from infected patients provided  
337 important information pertaining to ZIKV transmission (29). These data  
338 highlighted the degree of divergence in sequenced genomes and placed  
339 further emphasis on understanding virus evolution and transmission  
340 effectiveness (30). As not all recovered ZIKV RNA samples contained the  
341 same mutations, it will be interesting to determine how different host  
342 immune responses can lead to ZIKV quasi-species that acquire different  
343 combinations of mutations.

344 ZIKV infection led to the differential abundance of host transcripts  
345 mapping to numerous cellular genes in MDMs but not in monocytes, likely to  
346 be due to the higher levels of infection observed in MDMs. Furthermore, it is  
347 known that differences between donors can account for significant varied  
348 cellular responses (31,32), which when coupled with the lower infection  
349 levels observed in the monocytes may have triggered a disparate range of  
350 immune responses. However, this differential effect does not necessary  
351 signify that ZIKV-infected monocytes do not elicit any cellular response to  
352 infection, but rather the differences were not measurable by RNA-seq at the  
353 read depths used in this analysis. In fact, transcript abundance of numerous  
354 genes were different between the mock and ZIKV-infected monocytes, just  
355 that the statistical threshold of  $FDR < 0.05$  was not reached and was thus  
356 excluded from further analyses. Using IPA data mining, these differentially  
357 expressed genes were involved in 133 and 63 canonical cellular pathways  
358 (27 of them being shared) in MDMs at 24 and 72 hpi, respectively. The lower



359 number of cellular pathways identified in ZIKV-infected MDMs at the later 72  
360 hpi time-point suggests that certain cellular functions may be shut down post-  
361 infection (33). This effect could signify: (1) that the host cells conserve energy  
362 to focus only on essential pathways for survival; and/or (2) the host cells  
363 have succumbed to ZIKV infection, which leads to transcriptional shutdown in  
364 host cells.

365         Unsurprisingly, the IFN response was the most highly expressed  
366 signalling pathway of these common pathways at both time-points because  
367 of virus trigger (34). This observation was further complemented by the  
368 presence of few other IFN-related pathways. Observations were found for  
369 the next two most expressed pathways — pathogenesis of multiple  
370 sclerosis and crosstalk between NK cells moDCs cells — both of which  
371 involve NK cells. Although ZIKV infection has not been previously  
372 associated with multiple sclerosis due to the relatively new disease  
373 spectrum, other viral infections such as Epstein-Barr virus (35) and measles  
374 virus (36) have been linked.

375         CXCL9, CXCL10, CXCL11 and CCL5 (identified as the top genes in  
376 the pathway) are known chemokines to stimulate NK-cell activation (37,38).  
377 The increased transcript abundance of these immune mediators, coupled  
378 with others such as IL-15, is a strong indication that ZIKV-infected  
379 macrophages are primed to “communicate” with NK cells. Other recent  
380 studies have also provided evidence of communication between  
381 macrophages and NK cells (18). The increased abundance of TNFSF10  
382 and FAS transcripts in ZIKV-infected MDMs, could indicate priming of NK-  
383 cell mediated apoptosis (39). Interestingly, levels of typical NK cell-

384 activating cytokines, such as IL-12 (40,41) and IL-18 (42,43) were not  
385 differentially expressed in this study. However, mRNA levels of IL-23 and  
386 IL-27, two cytokines belonging to the family of IL-12 (44) with roles in NK-  
387 cell activation (45,46) were increased.

388 Immune-phenotyping of whole blood samples from ZIKV-infected  
389 patients revealed the presence of CD69<sup>+</sup>CD56<sup>+</sup> immune cells  
390 (predominantly the CD56<sup>+</sup> NK cells) (15), suggesting the possible priming of  
391 NK cells in ZIKV infection. The involvement of NK cells was thus explored  
392 *ex vivo* in human primary PBMCs. Interestingly, *ex vivo* culture alone led to  
393 an increase in the basal expression level of CD69 in CD56<sup>+</sup>CD94<sup>+</sup> NK cells,  
394 as previously reported (47). Furthermore, ZIKV infection resulted in reduced  
395 levels of CD69, which is a phenomenon also reported for the flavivirus tick-  
396 borne encephalitis virus infection in healthy donor NK cells (48). Moreover,  
397 NK cells behave differently *ex vivo* and *in vivo* (49), which may explain the  
398 different levels of CD69 detected in patients and in *ex vivo* ZIKV-infected  
399 NK cells. It was also reported in CD69-deficient mice that the activity of NK  
400 cells remains functional (50). High levels of key NK activation markers,  
401 including the degranulation marker CD107a and intracellular cytokine IFN $\gamma$   
402 indicate the higher activation status of NK cells. The activity of NK cells was  
403 directly dependent on the presence of CD14<sup>+</sup> monocytes. ZIKV infection of  
404 PBMCs depleted of CD14<sup>+</sup> monocytes significantly down-regulated the  
405 expression of the various NK-cell markers, demonstrating the functional role  
406 of monocytes as one of the key players for NK-cell stimulation. The data  
407 presented in this study are further supported by a recent publication in  
408 which ZIKV patients had high levels of IL-18, TNF $\alpha$  and IFN $\gamma$  (20) —

409 immune mediators associated with NK-cell function. The usage of SJL  
410 mice, which lack NK cells (51), as a model of ZIKV infection also suggest a  
411 protective role for these immune cell given that these animals succumbed  
412 to cortical malformations (52). Likewise, NK-cell-mediated immune  
413 response was significantly increased in healthy volunteers receiving a  
414 vaccination for the closely related yellow fever virus (53).

415           Interestingly, multiplex quantification of secreted immune mediators  
416 from *ex vivo* ZIKV-infected PBMCs provided an alternate perspective. IL-18  
417 and IFN $\gamma$ , two NK-cell related cytokines, were below detection limit.  
418 However, freshly isolated PBMCs stimulated with culture supernatants from  
419 ZIKV-infected PBMCs resulted in increased priming of NK cells, clearly  
420 indicating that the concoction of immune mediators are capable in driving  
421 NK-cell activation.

422           Nonetheless, the, depletion of CD14<sup>+</sup> monocytes would abrogate this  
423 activation as observed by the low levels of MCP-1, IL-1RA, VEGF-A,  
424 Eotaxin, GRO $\alpha$ , IFN $\alpha$  SDF-1 $\alpha$ , IP-10, IL-6, IL-1 $\alpha$ , IL-1 $\beta$ , IL-8, IL-21 and IL-  
425 10. The reduced levels of MCP-1 could also have a detrimental effect on  
426 NK-cell recruitment and priming (37,54), although MCP-1 and VEGF-A  
427 have been reported to drive the production of each other (55-57). The high  
428 levels of secreted IL1RA from ZIKV-infected PBMCs could also have  
429 participated in the increased priming of NK cells, as IL1RA is known to  
430 potentiate the effect of IL-2 stimulation of NK cells (58). Thus, the loss of  
431 detectable IL-2 after ZIKV infection in CD14-depleted PBMCs would further  
432 dwindle NK-cell priming. The presence of other immune mediators such as  
433 IL-6, IL-8, IL-10 and IP-10, SDF-1 $\alpha$ , GRO $\alpha$ , IL-1 $\alpha$  and IL-1 $\beta$  in ZIKV-

434 infected non-depleted PBMCs would further provide an inflammatory  
435 condition for cellular activation. While the levels of these immune mediators  
436 have been reported to be high in ZIKV patients (20), IL-10 and IP-10 have  
437 been demonstrated to contribute to cytolysis and activation of NK cells  
438 (37,59). Levels of LIF (60), IL-22 (61) and IL-31 (62) were high upon ZIKV  
439 infection, indicating their roles in regulating T cells during ZIKV infection  
440 (63). T cells can regulate NK-cell activity (64) and monocytes could  
441 indirectly mediate NK-cells functions through the T lymphocytes.

442         To conclude, through a systematic investigative workflow combining  
443 approaches exploring host cell transcriptomes and immunoproteomes, it was  
444 demonstrated that monocytes and macrophages do not act alone, but in  
445 conjunction with other immune cells to orchestrate a series of host immune  
446 response and drive disease progression. As such, a comprehensive  
447 understanding of immune-cell interaction will have important clinical  
448 implications for the design of novel therapeutics that can either dampen down  
449 or enhance a response as appropriate.

450 **Materials and Methods**

451 **Ethics approval and consent to participate.** Whole blood samples were  
452 collected from ZIKV-infected patients who were referred to the Communicable  
453 Disease Centre, Tan Tock Seng Hospital, Singapore. Blood was obtained  
454 from patients who provided written informed consent. The study protocol was  
455 approved by the SingHealth Centralized Institutional Review Board (CIRB  
456 Ref: 2016/2219). Blood samples were collected from healthy donors with  
457 written consent in accordance with guidelines from the Health Sciences  
458 Authority of Singapore (study approval number: NUS IRB: 10-250).

459

460 **Patient whole blood samples.** This study utilized whole blood samples  
461 obtained from patients admitted to the Communicable Disease Centre at Tan  
462 Tock Seng Hospital, Singapore from 27 August to 18 October 2016. Samples  
463 included in this study were collected during the acute phase (1-7 pio) of ZIKV  
464 infection. These patients were confirmed to be infected with ZIKV by reverse-  
465 transcription polymerase chain reaction (RT-PCR) performed on serum and  
466 urine samples obtained during their first visit to the clinic. Whole blood  
467 samples were collected in EDTA Vacutainer tubes (Becton Dickinson). Whole  
468 blood samples were also obtained from healthy volunteers as controls, which  
469 were confirmed to be negative for ZIKV RNA by RT-PCR.

470

471 **Virus preparation.** The ZIKV strain (accession KJ776791) used in this study  
472 was originally isolated from the French Polynesia outbreak in 2013 (65). The  
473 virus was propagated as previously described (8). Briefly, the virus was  
474 propagated by multiple passages in Vero-E6 cells (ATCC; CRL-1587) and

475 pre-cleared by centrifugation before storing at  $-80^{\circ}\text{C}$ . The virus titre was  
476 determined using standard plaque assays with Vero-E6 cells. Vero-E6 cells  
477 were regularly tested for mycoplasma contamination and were grown and  
478 passaged in Dulbecco's Modified Eagle Medium (DMEM; HyClone)  
479 supplemented with 10% (vol/vol) FBS. UV-inactivation of ZIKV was performed  
480 with the CL-1000 UV cross-linker (UVP) at intensity of  $100\text{mJ}/\text{cm}^2$  for 10  
481 minutes.

482

483 **Isolation and depletion of monocytes from human PBMCs.** Monocytes  
484 were prepared from fresh human PBMCs as previously described (8) and by  
485 gradient centrifugation using Ficoll-Paque density gradient media (GE  
486 Healthcare). Subsequently, monocytes were isolated using an indirect  
487 magnetic labelling system (Monocyte Isolation Kit II, Miltenyi Biotec). A direct  
488 magnetic labelling system (Human CD14<sup>+</sup> monocytes isolation kit 2,  
489 STEMCELL) was used for depletion of monocytes from PBMCs. The  
490 manufacturers' protocols were strictly adhered to for these procedures.

491

492 **Differentiation of monocytes into MDMs.** Isolated monocytes were  
493 differentiated into MDMs by plating in complete Iscove Modified Dulbecco's  
494 Medium (IMDM) (Hyclone) supplemented with 10% (vol/vol) heat-inactivated  
495 human serum (HS) (Sigma-Aldrich), which was replaced every 2 days. ZIKV  
496 infections were performed on monocytes and MDMs 5 days later, as  
497 described below.

498

499 *Virus infection.* ZIKV infections were performed at multiplicity of infection  
500 (MOI) 10. Each infection mix consisted of a virus suspension prepared in  
501 serum-free IMDM (Hyclone). The cells were incubated with the infection mix  
502 at 37°C and allowed to adsorb for 2 h with intermittent shaking before the  
503 virus inoculum was removed and replaced with complete IMDM supplemented  
504 with 10% (vol/vol) HS (Sigma-Aldrich). Cells were incubated at 37°C until  
505 harvesting at 24 and 72 hpi. The harvested cells for downstream total RNA  
506 isolation were stored at -80°C. A total of 140 µl of the infected cell suspension  
507 was used to quantify the viral load. For assessment of monocyte function in  
508 NK-cell activation during ZIKV infection, total human PBMCs and donor-  
509 corresponding CD14-depleted PBMCs were infected with ZIKV at MOI 10. In  
510 parallel, both PBMC fractions were stimulated with 10ng/ml  
511 lipopolysaccharide (LPS; Sigma) as a positive control to measure NK-cell  
512 activation. Cells were subsequently treated with 1X Brefeldin (eBioscience)  
513 and stained with CD107a (BD Pharmingen) 6 h before harvesting at 36 hpi.  
514 The viral load was quantified from 140 µl of the infected cell suspension.  
515 Negative controls were cells undergoing the same infection conditions in the  
516 absence of infectious ZIKV particles. These controls are referred to as mock-  
517 infected samples.

518

519 **PBMCs stimulation assay.** Fresh PBMCs were isolated as described above  
520 and subjected to stimulation with ZIKV-infected culture supernatants in a final  
521 ration of 1:10 in fresh IMDM (Hyclone) supplement with 10% (vol/vol) of HS  
522 (Sigma-Aldrich). Cells were subsequently treated with 1X Brefeldin

523 (eBioscience) and stained with CD107a (BD Pharmingen) 6 h before  
524 harvesting at 36 h for downstream antibodies staining.

525

526 **Viral RNA extraction and viral load analysis.** Viral RNA was extracted  
527 using a QIAamp® Viral RNA Mini Kit (QIAGEN), according to manufacturer's  
528 instructions. Quantification of ZIKV NS5 RNA was determined by quantitative  
529 real time-PCR (qRT-PCR) TaqMan assay (66) using a QuantiTect® Probe  
530 RT-PCR Kit (QIAGEN) in a 12.5 µl reaction volume. All reactions were  
531 performed on a 7900HT Fast Real-Time PCR System machine (Applied  
532 Biosciences).

533

534 **Total RNA extraction.** Total RNA was extracted using an RNeasy Mini Kit  
535 (QIAGEN) according to the manufacturer's instructions. The extracted total  
536 RNA was quantified on a Nanodrop 1000 spectrophotometer (Thermo Fisher  
537 Scientific).

538

539 **Flow cytometry and antibodies.** Detection of ZIKV antigen was carried out  
540 in a two-step indirect intracellular labelling process. Briefly, harvested cells  
541 were first fixed and permeabilized with FACS lysing solution (BD Biosciences)  
542 and FACS permeabilization solution 2 (BD Biosciences), respectively. Antigen  
543 staining was then performed with a flavivirus-specific mouse monoclonal  
544 antibody (clone 4G2) (Millipore) followed by secondary staining with a goat  
545 anti-mouse IgG F(ab')<sub>2</sub> antibody (Invitrogen). Cells were then specifically  
546 stained for the surface markers CD45 and CD14 (for ZIKV-infected  
547 monocytes and MDMs). Dead cells were excluded by staining with the



548 LIVE/DEAD Fixable Aqua Dead Cell Stain Kit (Life Technologies). For  
549 PBMCs, surface markers CD45, CD14, CD3, CD19 and CD56 were stained  
550 prior to intracellular staining (for ZIKV-infected PBMCs). For patient samples,  
551 100  $\mu$ l of whole blood was stained for the surface markers, CD45, CD56,  
552 CD94, CD16, CD69, CD107a, NKG2D and NKG2A. The stained cells were  
553 subsequently incubated with FACS lysing solution (BD Biosciences) to lyse  
554 the red blood cells. CD56<sup>+</sup> cells were first identified and were subsequently  
555 further defined with the CD94 surface marker to give three other subsets -  
556 CD56<sup>bright</sup>CD94<sup>hi</sup>, CD56<sup>dim</sup>CD94<sup>hi</sup> and CD56<sup>dim</sup>CD94<sup>lo</sup> (16). To specifically  
557 assess NK-cell activity *ex vivo*, PBMC fractions were stained for CD107a and  
558 various lineage markers (CD3, CD19, CD20 and CD14) (15) in addition to the  
559 panel of antibodies used for patient whole blood staining. The usage of  
560 lineage markers excludes the presence of non-NK cells in the ensuing  
561 analysis. Stained PBMCs were fixed and permeabilized as described above  
562 before intracellular staining of ZIKV antigen and IFN $\gamma$ .

563 All antibodies used were mouse anti-human and were obtained from  
564 BD Pharmingen (CD3, CD19, CD20, CD14, CD69, CD56, CD94, NKG2D,  
565 CD107a and IFN $\gamma$ ), Biolegend (CD16 and CD45) and Miltenyi Biotec  
566 (NKG2A). Data were acquired on a Fortessa flow cytometer (BD Biosciences)  
567 with BD FACSDiva<sup>TM</sup> software. Data analysis was performed using FlowJo  
568 version 9.3.2 software (Tree Star, Inc).

569

570 **Cytokines quantification using microbead-based immunoassay and data**  
571 **analyses.** Cytokine levels in supernatant obtained from mock and ZIKV-  
572 infected PBMCs were measured simultaneously using the ProcartaPlex<sup>TM</sup>

573 immunoassay (Thermo Fisher Scientific) detecting for 45 secreted cytokines,  
574 chemokines and growth factors including brain derived neurotropic factor  
575 (BDNF); Eotaxin/CCL11; epidermal growth factor (EGF); fibroblast growth  
576 factor 2 (FGF-2); granulocyte macrophage-colony stimulating factor (GM-  
577 CSF); growth-related oncogene (GRO) alpha/CXCL1; hepatocyte growth  
578 factor (HGF); nerve growth factor (67) beta; leukemia inhibitory factor (10);  
579 interferon (IFN) alpha; IFN gamma; interleukin (IL)-1 beta; IL-1 alpha; IL-1RA;  
580 IL-2; IL-4; IL-5; IL-6; IL-7; IL-8/CXCL8; IL-9; IL-10; IL-12p70; IL-13; IL-15; IL-  
581 17A; IL-18; IL-21; IL-22; IL-23; IL-27; IL-31; interferon-gamma induced protein  
582 (IP)-10/CXCL10; monocyte chemoattractant protein (MCP-1/CCL2);  
583 macrophage inflammatory protein (MIP)-1 alpha/CCL3; MIP-1 beta/CCL4;  
584 regulated on activation, normal T cell expressed and secreted  
585 (RANTES)/CCL5; stromal cell-derived factor (SDF)-1 alpha/CXCL12; tumor  
586 necrosis factor (TNF) alpha; TNF beta/LTA; Platelets-derived growth factor  
587 (PDGF)-BB; placental growth factor (PLGF); stem cell factor (SCF); vascular  
588 endothelial growth factor (VEGF)-A; VEGF-D. Preparation of samples,  
589 reagents and immunoassay procedures were performed according to  
590 manufacturers' instructions. Data were acquired using Luminex FlexMap 3D®  
591 instrument (Millipore) and analyzed using Bio-plex Manager™ 6.0 software  
592 (Bio-Rad) based on standard curves plotted through a five-parameter logistic  
593 curve setting. Levels of BDNF, FGF-2, HGF, NGF, IFN gamma, IL-4, IL-5, IL-  
594 7, IL-12p70, IL-13, IL-15, IL-18, RANTES, PDGF-BB, PLGF and VEGF-D  
595 were below detection limit and excluded for further analysis. Hierarchical  
596 clustering was done using TM4-MeV (<http://mev.tm4.org/>).  
597

598 **RNA-seq and differential gene expression analysis.** The general approach  
599 to RNA-seq and differential expression has been previously described  
600 (10,68), and is detailed in brief below.

601

602 **RNA-seq.** RNA samples were treated with DNase using an Ambion Turbo  
603 DNA-free Kit (Ambion), and then purified using Ampure XP beads  
604 (Agencourt). The DNase-treated RNA (2 ug) underwent Ribozero treatment  
605 using an Epicentre Ribo-Zero Gold Kit (Human/Rat/Mouse) (Epicentre) and  
606 re-purified on Ampure XP beads. Successful RNA depletion was verified  
607 using a Qubit (Thermo Fisher Scientific) and an Agilent 2100 Bioanalyzer  
608 (Agilent) and all of the depleted RNA was used as input material for the  
609 ScriptSeq v2 RNA-Seq Library Preparation protocol. RNA was amplified for  
610 14 cycles and the libraries were purified on Ampure XP beads. Each library  
611 was quantified using Qubit and the size distribution was assessed using the  
612 AATI Fragment Analyser (Advanced Analytical). These final libraries were  
613 pooled in equimolar amounts using the Qubit and Fragment Analyser data.  
614 The quantity and quality of each pool was assessed by the Fragment  
615 Analyser and subsequently by qPCR using the Illumina Library Quantification  
616 Kit (KAPA Biosystems) on a Light Cycler LC480II (Roche) according to  
617 manufacturer's instructions. The template DNA was denatured according to  
618 the protocol described in the Illumina cBot User guide and loaded at 12 pM  
619 concentration. Sequencing was carried out on three lanes of an Illumina  
620 HiSeq 2500 with version 4 chemistry, generating 2 × 125 bp paired-end reads.

621

622 **Bioinformatics Analysis.** Briefly, base calling and de-multiplexing of indexed  
623 reads was performed using CASAVA version 1.8.2 (Illumina) to produce 30  
624 samples from the five lanes of sequence data in fastq format. The raw fastq  
625 files were trimmed to remove the Illumina adapter sequences using Cutadapt  
626 version 1.2.1 (69). The option “-O 3” was set so that the 3' end of any read  
627 that matched the adapter sequence by  $\geq 3$  bp was removed. The reads were  
628 further trimmed to remove low-quality bases using Sickle version 1.200 with a  
629 minimum window quality score of 20. After trimming, reads  $< 50$  bp were  
630 removed. If both reads from a pair passed this filter, each read was included  
631 in the R1 (forward reads) or R2 (reverse reads) file. If only one read of a read  
632 pair passed this filter, it was included in the R0 (unpaired reads) file. The  
633 reference genome used for alignment was the human reference genome  
634 assembly GRCh38. The reference sequence was downloaded from the  
635 Ensembl ftp site  
636 ([ftp://ftp.ensembl.org/pub/release77/fasta/homo\\_sapiens/dna/Homo\\_sapiens](ftp://ftp.ensembl.org/pub/release77/fasta/homo_sapiens/dna/Homo_sapiens)  
637 [GRCh38.dna\\_sm.primary\\_assembly.fa.gz](ftp://ftp.ensembl.org/pub/release77/fasta/homo_sapiens/dna/Homo_sapiens)). The reference annotation was  
638 also downloaded from the Ensembl ftp site (<ftp://ftp.ensembl.org/pub/release->  
639 [77/gtf/homo\\_sapiens/Homo\\_sapiens.GRCh38.77.gtf.gz](ftp://ftp.ensembl.org/pub/release-77/gtf/homo_sapiens/Homo_sapiens.GRCh38.77.gtf.gz)). The annotated file  
640 contained 63,152 genes. R1/R2 read pairs were mapped to the reference  
641 sequence using TopHat2 version 2.1.0 (70) that employs the mapper Bowtie2  
642 version 2.0.10 (71).

643

644 **Differential Gene Expression and Functional Analysis.** Mapped reads  
645 were further analyzed using EdgeR version 3.3 (72) to calculate normalized  
646 counts per million (CPM), identify differentially expressed genes between

647 infected and mock-infected conditions, and compare infected conditions with  
648 each other. Correlation and PCA analysis plots were created in RStudio.  
649 Heat-maps were generated using GENE-E (Broad Institute;  
650 <https://software.broadinstitute.org/GENE-E/>). IPA was used for gene ontology  
651 and pathway analysis. The *P* value associated with each identified canonical  
652 pathway was calculated by Fisher's Exact test (right-tailed). The presence of  
653 the 27 common canonical pathways was illustrated in a heat-map generated  
654 by hierarchical clustering using TM4-MeV (73).

655

656 **Identification of ZIKV variants.** Bowtie 2 (71) was used to determine the  
657 mean sequence coverage. Here, 12 of the 41 samples (including the  
658 inoculum) had a mean coverage >10 following alignment with the ZIKV  
659 reference genome (accession KJ776791) used in this study. The frequencies  
660 of minor variants were calculated using QuasiRecomb (74). Sequences of  
661 individual viral proteins were compared to the protein databank using the  
662 online NCBI Protein BLAST server  
663 (<https://blast.ncbi.nlm.nih.gov/Blast.cgi?PAGE=Proteins>).

664

665 **Author contributions**

666 FML, DAM, JAH and LFPN designed the study. FML, DL, DAM, JAH and  
667 LFPN wrote the manuscript. FML, CTK, CLYP, JJLT, XL, WXY and YXF  
668 performed the experiments. FML, DL, XL, YXF, BL, NYR, DAM, JAH and  
669 LFPN analysed the data. All other authors were involved in sample collection,  
670 processing and analysis, and/or logistical support. All authors read and  
671 approved the final manuscript.

672 **Acknowledgements**

673 The authors would like to thank Siti Naqiah Amrun, Yiu-Wing Kam, Jonathan  
674 Cox, Yi-Hao Chan, Guillaume Carissimo, Farhana Abu Bakar, Nicholas Q.R.  
675 Kng, Kia-Joo Puan and Nurhashikin Binte Yusof from SIgN for their help in the  
676 processing of patient samples. The authors also thank Linda Kay Lee from the  
677 Communicable Diseases Centre and Ivy Low, Seri Mustafah and Anis Larbi  
678 from the SIgN Flow Cytometry team for their assistance. The authors are  
679 grateful to all patients and healthy volunteers for their participation in the  
680 study. Finally, the authors would like to thank Laurent Rénia and Insight  
681 Editing London for comments and proofreading the manuscript prior to  
682 submission. This work was supported by core research grants provided to the  
683 Singapore Immunology Network (SIgN) by the Biomedical Research Council  
684 (BMRC) and by the BMRC A\*STAR-led Zika Virus Consortium Fund [project  
685 number: 15/1/82/27/001], Agency for Science, Technology and Research  
686 (A\*STAR), Singapore. This work was also supported by funds provided by the  
687 Medical Research Council (MRC) [project number: MC\_PC\_15094], and by  
688 the HPRU in Emerging and Zoonotic Infections Cross NIHR Strategic  
689 Research Fund [project number: ZLKN\_11447], United Kingdom. The views  
690 expressed are those of the author(s) and not necessarily those of the  
691 A\*STAR, NHS, the NIHR, the Department of Health or PHE.

692 **References**

- 693 1. Korzeniewski, K, Juszczak, D , Zwolinska, E. Zika - another threat on  
694 the epidemiological map of the world. *Int Marit Health*. 2016;67(1):31-7.
- 695 2. Dick, GW, Kitchen, SF , Haddow, AJ. Zika virus. I. Isolations and  
696 serological specificity. *Trans R Soc Trop Med Hyg*. 1952;46(5):509-20.
- 697 3. Duffy, MR et al. Zika virus outbreak on Yap Island, Federated States of  
698 Micronesia. *N Engl J Med*. 2009;360(24):2536-43.
- 699 4. Cao-Lormeau, VM et al. Guillain-Barre Syndrome outbreak associated  
700 with Zika virus infection in French Polynesia: a case-control study.  
701 *Lancet*. 2016;387(10027):1531-9.
- 702 5. Brasil, P et al. Zika Virus Infection in Pregnant Women in Rio de  
703 Janeiro - Preliminary Report. *N Engl J Med*. 2016  
704 doi:10.1056/NEJMoa1602412.
- 705 6. Foo, SS et al. Asian Zika virus strains target CD14+ blood monocytes  
706 and induce M2-skewed immunosuppression during pregnancy. *Nat*  
707 *Microbiol*. 2017 doi:10.1038/s41564-017-0016-3.
- 708 7. Lum, FM et al. Sensitive detection of Zika virus antigen in patients'  
709 whole blood as an alternative diagnostic approach. *J Infect Dis*. 2017  
710 doi:10.1093/infdis/jix276.
- 711 8. Lum, FM et al. Zika Virus Infects Human Fetal Brain Microglia and  
712 Induces Inflammation. *Clin Infect Dis*. 2017;64(7):914-20.



- 713 9. Michlmayr, D, Andrade, P, Gonzalez, K, Balmaseda, A , Harris, E.  
714 CD14+CD16+ monocytes are the main target of Zika virus infection in  
715 peripheral blood mononuclear cells in a paediatric study in Nicaragua.  
716 *Nat Microbiol.* 2017 doi:10.1038/s41564-017-0035-0.
- 717 10. Liu, X et al. Transcriptomic signatures differentiate survival from fatal  
718 outcomes in humans infected with Ebola virus. *Genome Biol.*  
719 2017;18(1):4.
- 720 11. Bowen, JR et al. Zika Virus Antagonizes Type I Interferon Responses  
721 during Infection of Human Dendritic Cells. *PLoS Pathog.*  
722 2017;13(2):e1006164.
- 723 12. Carroll, MW et al. Temporal and spatial analysis of the 2014-2015  
724 Ebola virus outbreak in West Africa. *Nature.* 2015;524(7563):97-101.
- 725 13. Dowall, SD et al. Elucidating variations in the nucleotide sequence of  
726 Ebola virus associated with increasing pathogenicity. *Genome Biol.*  
727 2014;15(11):540.
- 728 14. Singapore Zika Study, G. Outbreak of Zika virus infection in Singapore:  
729 an epidemiological, entomological, virological, and clinical analysis.  
730 *Lancet Infect Dis.* 2017;17(8):813-21.
- 731 15. Montaldo, E et al. Human NK cell receptors/markers: a tool to analyze  
732 NK cell development, subsets and function. *Cytometry A.*  
733 2013;83(8):702-13.

- 734 16. Yu, J et al. CD94 surface density identifies a functional intermediary  
735 between the CD56bright and CD56dim human NK-cell subsets. *Blood*.  
736 2010;115(2):274-81.
- 737 17. Fogel, LA, Sun, MM, Geurs, TL, Carayannopoulos, LN , French, AR.  
738 Markers of nonselective and specific NK cell activation. *J Immunol*.  
739 2013;190(12):6269-76.
- 740 18. Michel, T, Hentges, F , Zimmer, J. Consequences of the crosstalk  
741 between monocytes/macrophages and natural killer cells. *Front*  
742 *Immunol*. 2012;3:403.
- 743 19. Marcais, A et al. The metabolic checkpoint kinase mTOR is essential  
744 for IL-15 signaling during the development and activation of NK cells.  
745 *Nat Immunol*. 2014;15(8):749-57.
- 746 20. Kam, YW et al. Specific Biomarkers Associated With Neurological  
747 Complications and Congenital Central Nervous System Abnormalities  
748 From Zika Virus-Infected Patients in Brazil. *J Infect Dis*.  
749 2017;216(2):172-81.
- 750 21. El Costa, H et al. ZIKA virus reveals broad tissue and cell tropism  
751 during the first trimester of pregnancy. *Sci Rep*. 2016;6:35296.
- 752 22. Hamel, R et al. Biology of Zika Virus Infection in Human Skin Cells. *J*  
753 *Virol*. 2015;89(17):8880-96.
- 754 23. Quicke, KM et al. Zika Virus Infects Human Placental Macrophages.  
755 *Cell Host Microbe*. 2016;20(1):83-90.

- 756 24. Gordon, S, Pluddemann, A , Martinez Estrada, F. Macrophage  
757 heterogeneity in tissues: phenotypic diversity and functions. *Immunol*  
758 *Rev.* 2014;262(1):36-55.
- 759 25. Gordon, S , Taylor, PR. Monocyte and macrophage heterogeneity. *Nat*  
760 *Rev Immunol.* 2005;5(12):953-64.
- 761 26. Martinez, FO, Gordon, S, Locati, M , Mantovani, A. Transcriptional  
762 profiling of the human monocyte-to-macrophage differentiation and  
763 polarization: new molecules and patterns of gene expression. *J*  
764 *Immunol.* 2006;177(10):7303-11.
- 765 27. Ploeger, DT et al. Cell plasticity in wound healing: paracrine factors of  
766 M1/ M2 polarized macrophages influence the phenotypical state of  
767 dermal fibroblasts. *Cell Commun Signal.* 2013;11(1):29.
- 768 28. Italiani, P , Boraschi, D. From Monocytes to M1/M2 Macrophages:  
769 Phenotypical vs. Functional Differentiation. *Front Immunol.* 2014;5:514.
- 770 29. Grubaugh, ND et al. Genomic epidemiology reveals multiple  
771 introductions of Zika virus into the United States. *Nature.* 2017  
772 doi:10.1038/nature22400.
- 773 30. Rodpothong, P , Auewarakul, P. Viral evolution and transmission  
774 effectiveness. *World J Virol.* 2012;1(5):131-4.
- 775 31. Mamrut, S et al. Integrative analysis of methylome and transcriptome in  
776 human blood identifies extensive sex- and immune cell-specific  
777 differentially methylated regions. *Epigenetics.* 2015;10(10):943-57.

- 778 32. Wong, KL et al. Gene expression profiling reveals the defining features  
779 of the classical, intermediate, and nonclassical human monocyte  
780 subsets. *Blood*. 2011;118(5):e16-31.
- 781 33. Carrasco, L. The inhibition of cell functions after viral infection. A  
782 proposed general mechanism. *FEBS Lett*. 1977;76(1):11-5.
- 783 34. Randall, RE , Goodbourn, S. Interferons and viruses: an interplay  
784 between induction, signalling, antiviral responses and virus  
785 countermeasures. *J Gen Virol*. 2008;89(Pt 1):1-47.
- 786 35. Lunemann, JD. Epstein-Barr virus in multiple sclerosis: a continuing  
787 conundrum. *Neurology*. 2012;78(1):11-2.
- 788 36. Tucker, WG , Andrew Paskauskas, R. The MSMV hypothesis: measles  
789 virus and multiple sclerosis, etiology and treatment. *Med Hypotheses*.  
790 2008;71(5):682-9.
- 791 37. Robertson, MJ. Role of chemokines in the biology of natural killer cells.  
792 *J Leukoc Biol*. 2002;71(2):173-83.
- 793 38. Thapa, M, Welner, RS, Pelayo, R , Carr, DJ. CXCL9 and CXCL10  
794 expression are critical for control of genital herpes simplex virus type 2  
795 infection through mobilization of HSV-specific CTL and NK cells to the  
796 nervous system. *J Immunol*. 2008;180(2):1098-106.
- 797 39. Warren, HS , Smyth, MJ. NK cells and apoptosis. *Immunol Cell Biol*.  
798 1999;77(1):64-75.

- 799 40. Kobayashi, M et al. Identification and purification of natural killer cell  
800 stimulatory factor (NKSF), a cytokine with multiple biologic effects on  
801 human lymphocytes. *J Exp Med.* 1989;170(3):827-45.
- 802 41. Liu, J et al. Interleukin-12: an update on its immunological activities,  
803 signaling and regulation of gene expression. *Curr Immunol Rev.*  
804 2005;1(2):119-37.
- 805 42. French, AR, Holroyd, EB, Yang, L, Kim, S , Yokoyama, WM. IL-18 acts  
806 synergistically with IL-15 in stimulating natural killer cell proliferation.  
807 *Cytokine.* 2006;35(5-6):229-34.
- 808 43. Takeda, K et al. Defective NK cell activity and Th1 response in IL-18-  
809 deficient mice. *Immunity.* 1998;8(3):383-90.
- 810 44. Kastelein, RA, Hunter, CA , Cua, DJ. Discovery and biology of IL-23  
811 and IL-27: related but functionally distinct regulators of inflammation.  
812 *Annu Rev Immunol.* 2007;25:221-42.
- 813 45. Matsui, M et al. Interleukin-27 activates natural killer cells and  
814 suppresses NK-resistant head and neck squamous cell carcinoma  
815 through inducing antibody-dependent cellular cytotoxicity. *Cancer Res.*  
816 2009;69(6):2523-30.
- 817 46. van de Wetering, D, de Paus, RA, van Dissel, JT , van de Vosse, E. IL-  
818 23 modulates CD56+/CD3- NK cell and CD56+/CD3+ NK-like T cell  
819 function differentially from IL-12. *Int Immunol.* 2009;21(2):145-53.

- 820 47. Kim, TJ et al. Homotypic NK cell-to-cell communication controls  
821 cytokine responsiveness of innate immune NK cells. *Sci Rep.*  
822 2014;4:7157.
- 823 48. Krylova, NV, Smolina, TP , Leonova, GN. Molecular Mechanisms of  
824 Interaction Between Human Immune Cells and Far Eastern Tick-Borne  
825 Encephalitis Virus Strains. *Viral Immunol.* 2015;28(5):272-81.
- 826 49. Gotlieb, N et al. The misleading nature of in vitro and ex vivo findings in  
827 studying the impact of stress hormones on NK cell cytotoxicity. *Brain*  
828 *Behav Immun.* 2015;45:277-86.
- 829 50. Notario, L, Alari-Pahissa, E, de Molina, A , Lauzurica, P. CD69  
830 Deficiency Enhances the Host Response to Vaccinia Virus Infection  
831 through Altered NK Cell Homeostasis. *J Virol.* 2016;90(14):6464-74.
- 832 51. Sellers, RS, Clifford, CB, Treuting, PM , Brayton, C. Immunological  
833 variation between inbred laboratory mouse strains: points to consider in  
834 phenotyping genetically immunomodified mice. *Vet Pathol.*  
835 2012;49(1):32-43.
- 836 52. Cugola, FR et al. The Brazilian Zika virus strain causes birth defects in  
837 experimental models. *Nature.* 2016;534(7606):267-71.
- 838 53. Gaucher, D et al. Yellow fever vaccine induces integrated multilineage  
839 and polyfunctional immune responses. *J Exp Med.* 2008;205(13):3119-  
840 31.

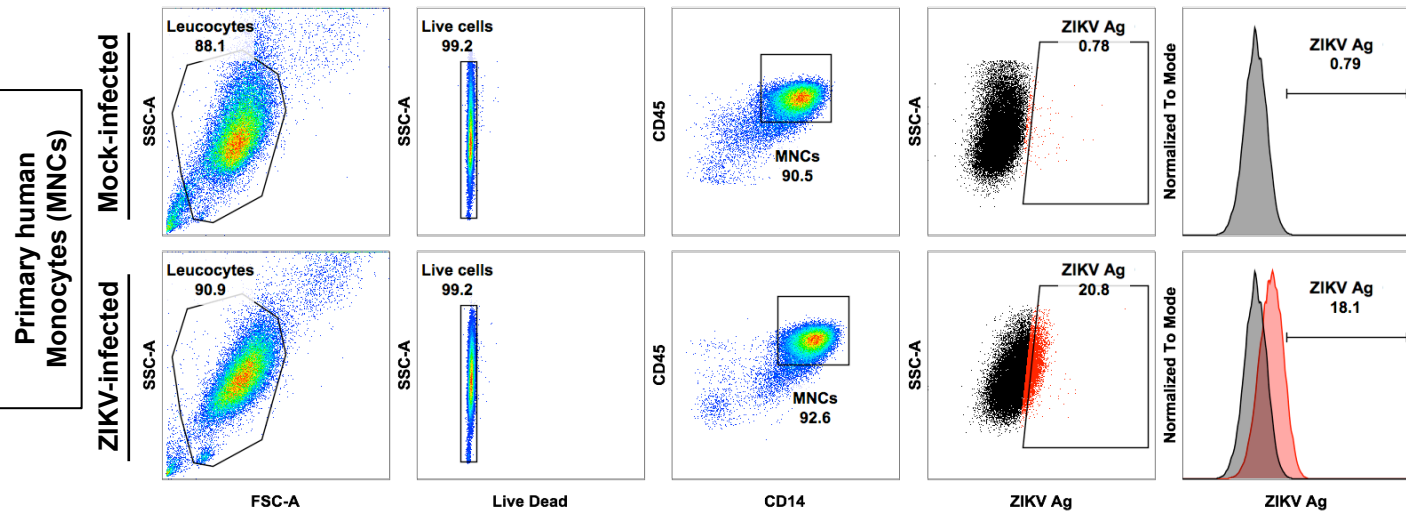
- 841 54. Morrison, BE, Park, SJ, Mooney, JM , Mehrad, B. Chemokine-  
842 mediated recruitment of NK cells is a critical host defense mechanism  
843 in invasive aspergillosis. *J Clin Invest.* 2003;112(12):1862-70.
- 844 55. Eubank, TD, Galloway, M, Montague, CM, Waldman, WJ , Marsh, CB.  
845 M-CSF induces vascular endothelial growth factor production and  
846 angiogenic activity from human monocytes. *J Immunol.*  
847 2003;171(5):2637-43.
- 848 56. Kuroda, T et al. Monocyte chemoattractant protein-1 transfection  
849 induces angiogenesis and tumorigenesis of gastric carcinoma in nude  
850 mice via macrophage recruitment. *Clin Cancer Res.* 2005;11(21):7629-  
851 36.
- 852 57. Marumo, T, Schini-Kerth, VB , Busse, R. Vascular endothelial growth  
853 factor activates nuclear factor-kappaB and induces monocyte  
854 chemoattractant protein-1 in bovine retinal endothelial cells. *Diabetes.*  
855 1999;48(5):1131-7.
- 856 58. Conti, P et al. Activation of human natural killer cells by  
857 lipopolysaccharide and generation of interleukin-1 alpha, beta, tumour  
858 necrosis factor and interleukin-6. Effect of IL-1 receptor antagonist.  
859 *Immunology.* 1991;73(4):450-6.
- 860 59. Park, JY et al. IL-15-induced IL-10 increases the cytolytic activity of  
861 human natural killer cells. *Mol Cells.* 2011;32(3):265-72.
- 862 60. Metcalfe, SM. LIF in the regulation of T-cell fate and as a potential  
863 therapeutic. *Genes Immun.* 2011;12(3):157-68.

- 864 61. Wolk, K, Kunz, S, Asadullah, K , Sabat, R. Cutting edge: immune cells  
865 as sources and targets of the IL-10 family members? *J Immunol.*  
866 2002;168(11):5397-402.
- 867 62. Zhang, Q, Putheti, P, Zhou, Q, Liu, Q , Gao, W. Structures and  
868 biological functions of IL-31 and IL-31 receptors. *Cytokine Growth*  
869 *Factor Rev.* 2008;19(5-6):347-56.
- 870 63. Elong Ngono, A et al. Mapping and Role of the CD8+ T Cell Response  
871 During Primary Zika Virus Infection in Mice. *Cell Host Microbe.*  
872 2017;21(1):35-46.
- 873 64. Kerdiles, Y, Ugolini, S , Vivier, E. T cell regulation of natural killer cells.  
874 *J Exp Med.* 2013;210(6):1065-8.
- 875 65. Baronti, C et al. Complete coding sequence of zika virus from a French  
876 polynesia outbreak in 2013. *Genome Announc.* 2014;2(3).
- 877 66. Balm, MN et al. A diagnostic polymerase chain reaction assay for Zika  
878 virus. *J Med Virol.* 2012;84(9):1501-5.
- 879 67. Wu, D et al. Chikungunya outbreak in Guangdong Province, China,  
880 2010. *Emerging infectious diseases.* 2012;18(3):493-5.
- 881 68. Bosworth, A et al. A comparison of host gene expression signatures  
882 associated with infection in vitro by the Makona and Ecran (Mayinga)  
883 variants of Ebola virus. *Sci Rep.* 2017;7:43144.
- 884 69. Tang, H et al. Zika Virus Infects Human Cortical Neural Progenitors  
885 and Attenuates Their Growth. *Cell Stem Cell.* 2016;18(5):587-90.

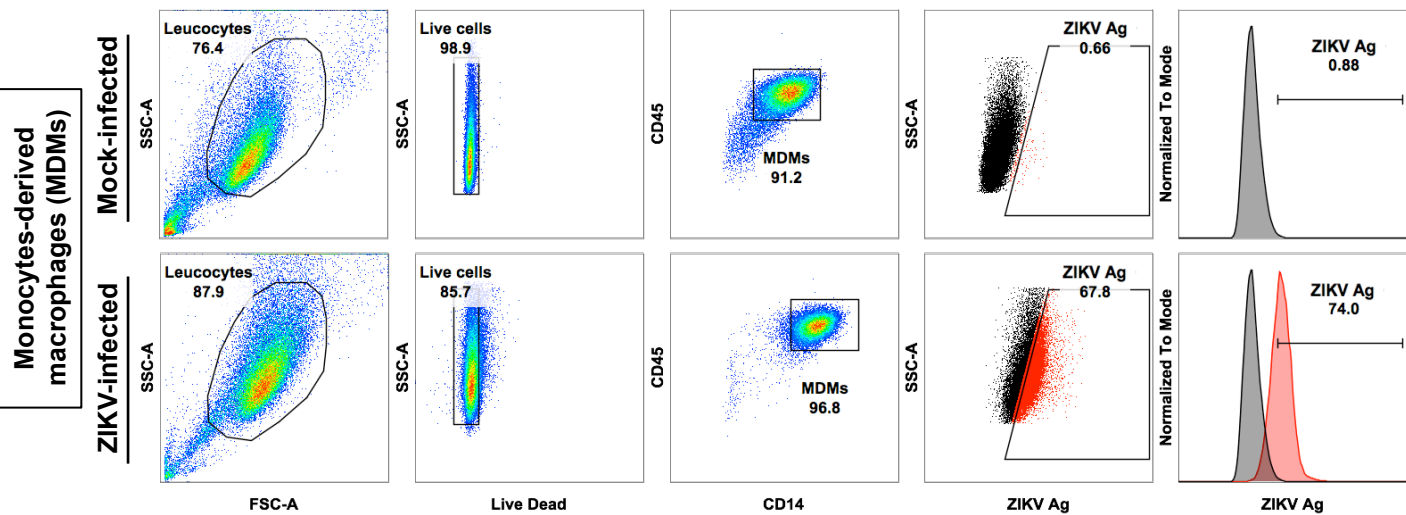


- 886 70. Kim, D et al. TopHat2: accurate alignment of transcriptomes in the  
887 presence of insertions, deletions and gene fusions. *Genome Biol.*  
888 2013;14(4):R36.
- 889 71. Langmead, B , Salzberg, SL. Fast gapped-read alignment with Bowtie  
890 2. *Nat Methods.* 2012;9(4):357-9.
- 891 72. Robinson, MD, McCarthy, DJ , Smyth, GK. edgeR: a Bioconductor  
892 package for differential expression analysis of digital gene expression  
893 data. *Bioinformatics.* 2010;26(1):139-40.
- 894 73. Saeed, AI et al. TM4: a free, open-source system for microarray data  
895 management and analysis. *Biotechniques.* 2003;34(2):374-8.
- 896 74. Beerenwinkel, N , Zagordi, O. Ultra-deep sequencing for the analysis of  
897 viral populations. *Curr Opin Virol.* 2011;1(5):413-8.  
898

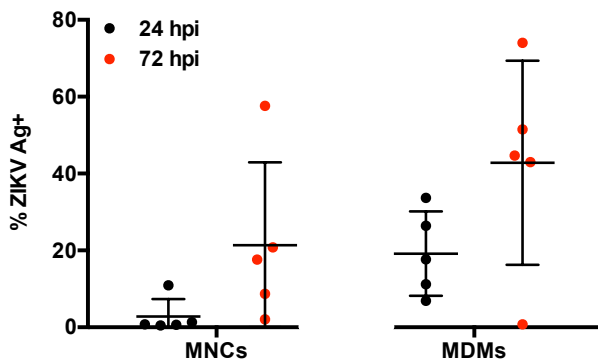
**A**



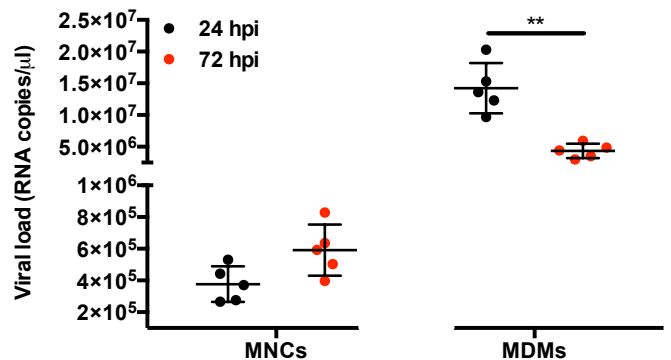
**B**



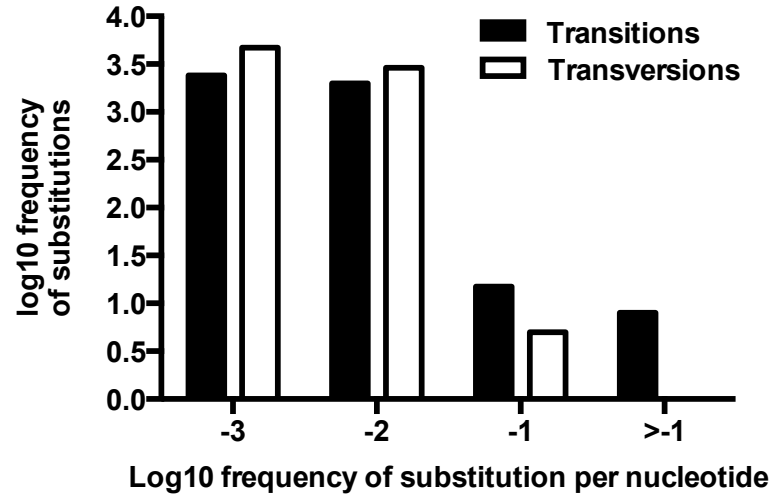
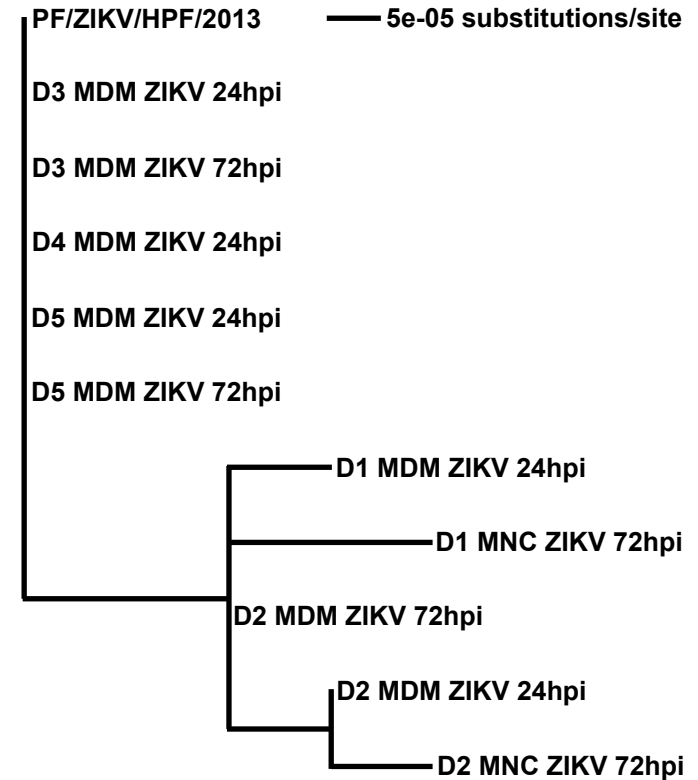
**C**



**D**

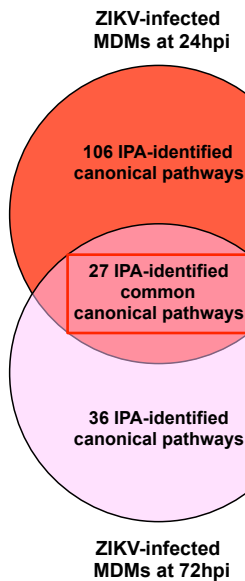


**Figure 1: Primary human MNCs and MDMs are targets of ZIKV infection.** Isolated human primary MNCs and MDMs ( $2 \times 10^6$  cells each) were infected with ZIKV at MOI 10 and harvested at 24 and 72 hpi. Flow cytometry gating on **(A)** monocytes (MNCs) and **(B)** MDMs. Gating for positive infection was set using the mock-infected samples. For the dot plots, cells positive for ZIKV Ag are shown in red. For the histogram, ZIKV-infected samples (red) were overlaid on mock-infected samples (black). Compiled results for **(C)** infection (ZIKV Ag) and **(D)** viral load detected in MNCs and MDMs obtained from five healthy donors. All data are presented as mean  $\pm$  SD. \* $P < 0.05$ , by Mann Whitney  $U$  test, two tailed. Viral load data was not statistically significant between 24 and 72 hpi in MNCs by Mann Whitney  $U$  test, two tailed. Abbreviations: hpi, hours post-infection; MDM, monocyte-derived macrophage; MNC, monocyte; ZIKV, Zika virus; Ag, antigen.

**A****B**

**Figure 2: Phylogenetic analyses based on sample consensus sequences.** (A) Frequency of ZIKV minor variants (transitions and transversions) recovered from infected human primary MNCs and MDMs isolated from five donors. Bin -3 is where  $\leq 1/1000$  reads show a specific change at an individual nucleotide position. Bin -2 is  $> 1/1000$  and  $\leq 1/100$  reads showing a difference. Bin -1 is  $> 1/100$  and  $\leq 1/10$  reads and Bin  $> -1$  is  $> 1/10$  reads showing a change up to a logical limit of just under  $\frac{1}{2}$ . (B) Phylogenetic tree generated from the alignment of consensus sequences of ZIKV RNA recovered from the same samples as described in (A). All samples included in the tree had a mean sequence coverage  $> 10$  at each nucleotide position. PF/ZIKV/HPF/2013 is the virus strain used for infection and denoted as the reference sample in this analysis. Abbreviations: hpi, hours post-infection; MDM, monocyte-derived macrophage; MNC, monocyte; ZIKV, Zika virus.

**A**



24 hpi	72 hpi	
**	**	Activation of IRF by cytosolic pattern recognition receptors
*	*	Acute phase response signalling
*	*	Agranulocyte adhesion and diapedesis
***	*	Antigen presentation pathway
**	**	Communication between innate and adaptive immune cells
**	**	Crosstalk between dendritic cells and natural killer cells
**	*	Death receptor signalling
**	**	Fcy receptor-mediated phagocytosis in macrophages and monocytes
*	*	IL-10 signalling
**	*	Granulocyte adhesion and diapedesis
*	*	IL-15 production
*	**	iNOS signalling
***	***	Interferon signalling
*	*	Mitochondrial dysfunction

24 hpi	72 hpi	
*	*	Pancreatic adenocarcinoma signalling
***	**	Pathogenesis of multiple sclerosis
*	**	Production of nitric oxide and reactive oxygen species in macrophages
**	*	Retinoic acid mediated apoptosis signalling
*	*	Role of BRCA1 in DNA damage response
*	*	Role of hypercytokinemia/hyperchemokinaemia in the pathogenesis of Influenza
*	*	Role of JAK1, JAK2 and TYK2 in interferon signalling
**	*	Role of pattern recognition receptors in recognition of bacteria and viruses
*	*	Role of RIG-I like receptors in antiviral innate immunity
*	*	T helper cell differentiation
*	*	Tec kinase signalling
*	**	TREM1 signalling
*	*	Type I diabetes mellitus signalling

\*P value < 0.05; \*\*P value < 1x10<sup>-3</sup>; \*\*\*P value 1x10<sup>-6</sup>

Low abundance High abundance

**B**

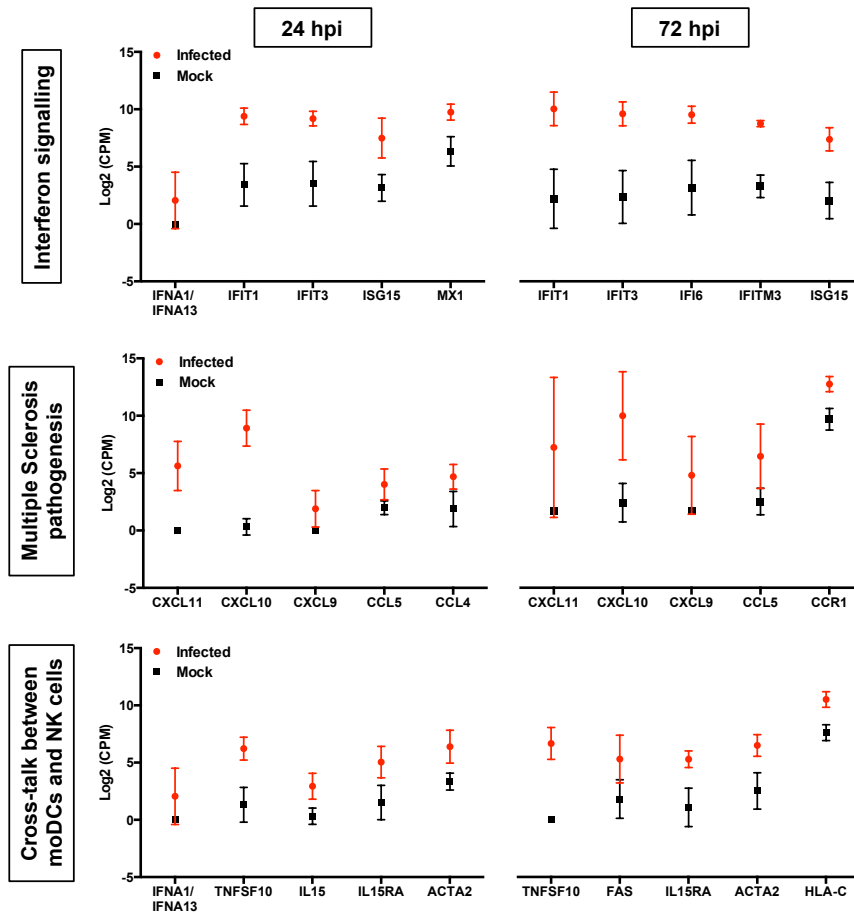
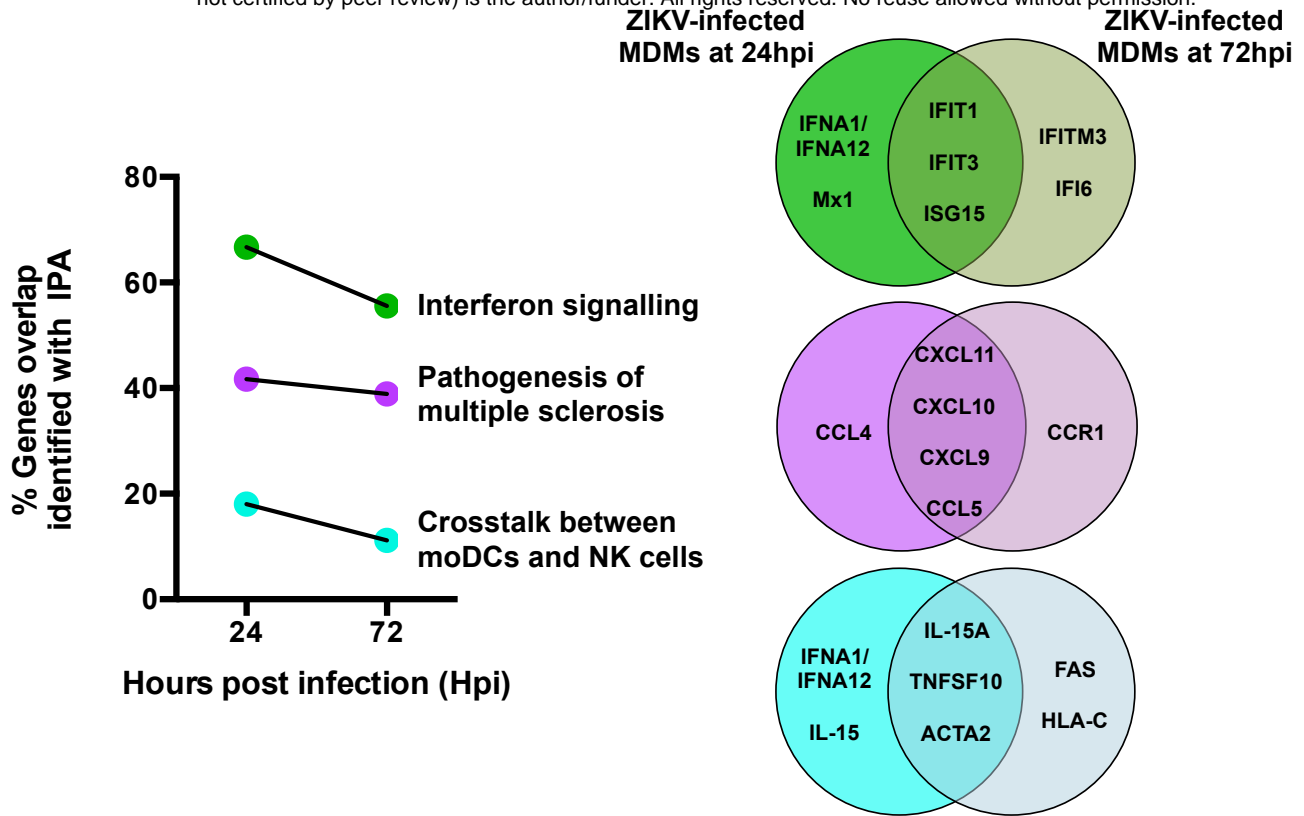


**Figure 3: Transcriptomic profiling of host cells during ZIKV infection.** Primary human MNCs and MDMs ( $2 \times 10^6$  cells per infection) were infected with ZIKV at MOI 10 and harvested at 24 and 72 hpi for transcriptomic analysis by RNA-seq and then compared to mock-infected controls. **(A)** Venn-diagram illustrating the proportion of up-regulated signaling pathways identified by IPA in ZIKV-infected MDMs. Up-regulation intensity of the 27 common canonical pathways are shown in a heat-map. Stars within the boxes represent the calculated *P* values associated with each identified pathway, compared to the mock-infected samples. **(B)** The five most up-regulated genes within the top three signaling pathways at 24 and 72 hpi are shown: Interferon pathway, multiple sclerosis pathway and crosstalk between moDCs and NK cells. Data presented were obtained from a total of five donors. Abbreviations: hpi, hours post-infection; NK, natural killer; IPA, ingenuity pathway analysis; MDM, monocyte-derived macrophage; MNC, monocyte; moDCs, monocyte-derived dendritic cells; ZIKV, Zika virus.

**A**



**B**

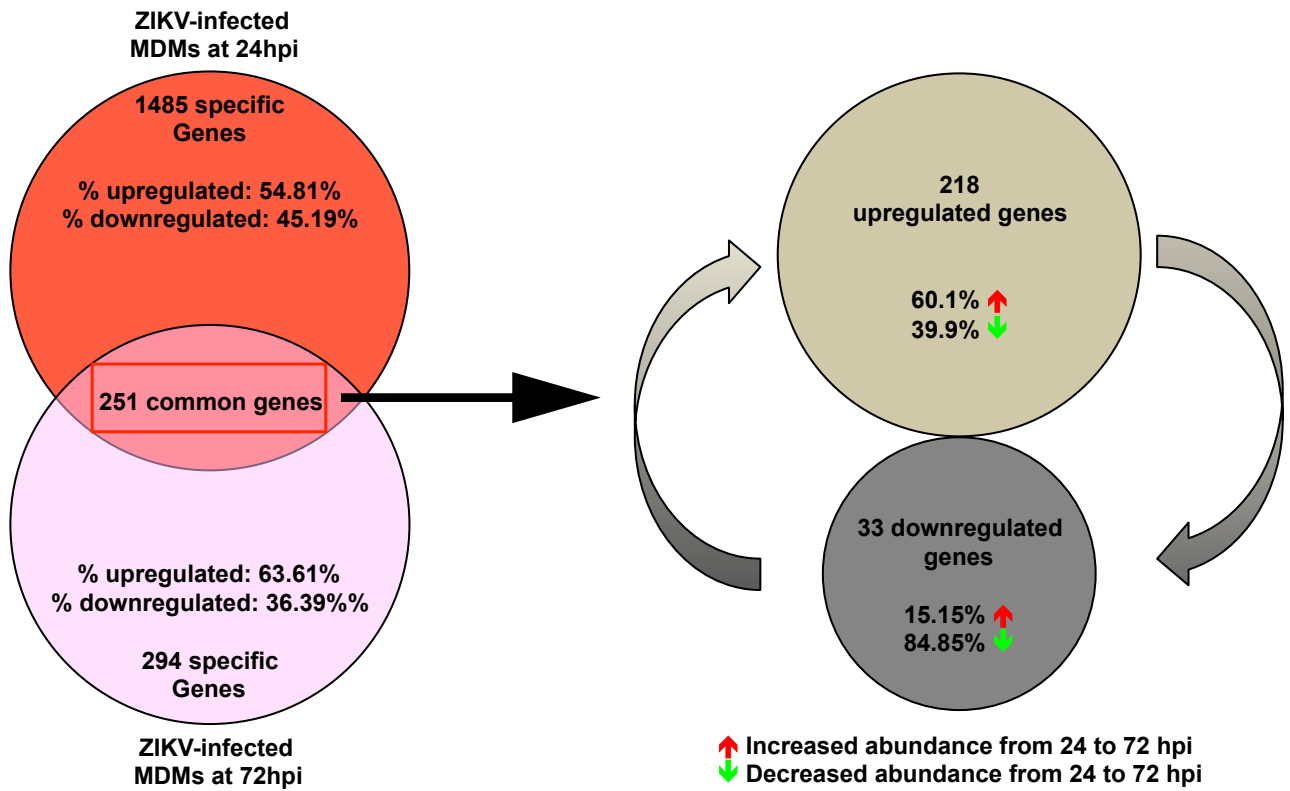
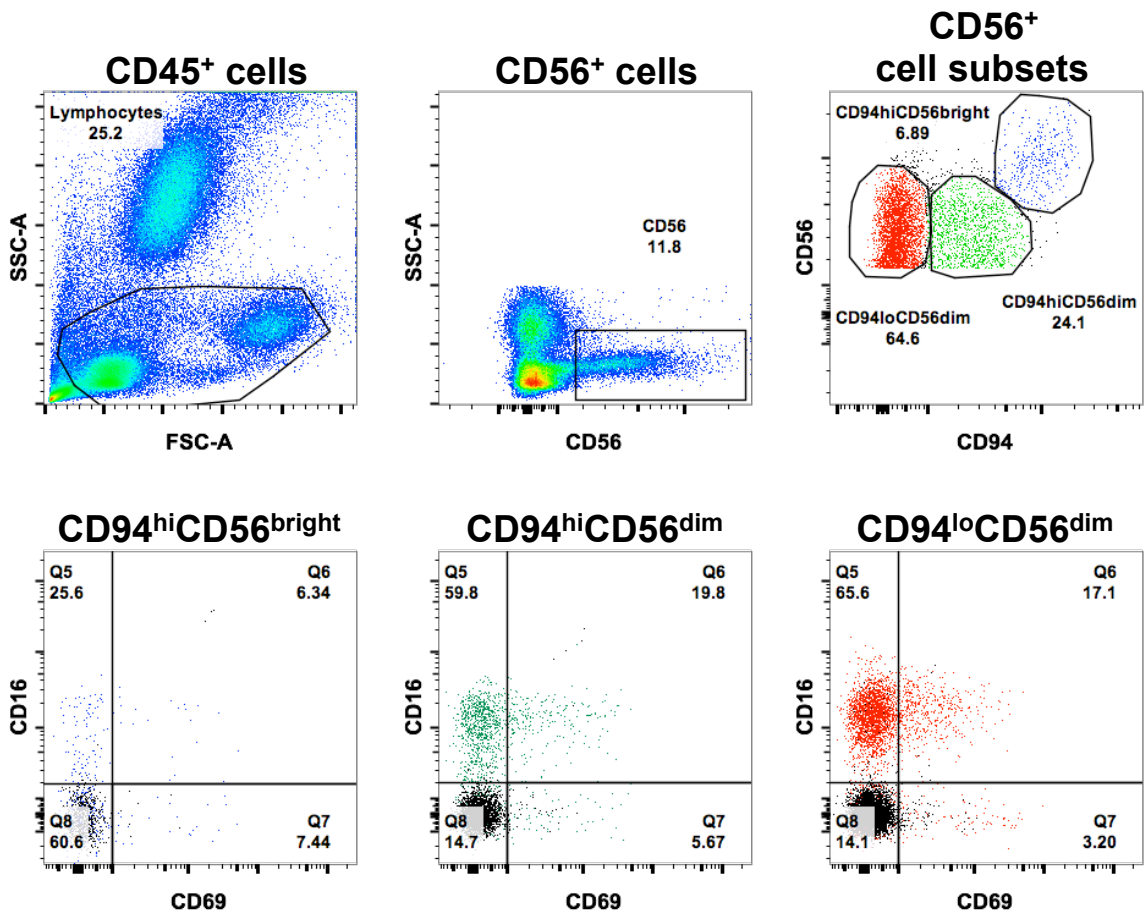


**Figure 4: Transition of the host cellular response over the course of ZIKV infection.** The host cellular response was analyzed and investigated by RNA-sequencing and significant transcriptomic differences were identified. (A) Transitional analysis (% genes overlapping) of the top three common canonical signaling pathways was determined using IPA of infected MDMs. Venn diagrams indicate the top five common and time-point specific genes associated with each canonical pathway. (B) Proportion of common and differentially expressed genes within ZIKV-infected MDMs at 24 and 72 hpi. Data presented were obtained from a total of five donors. Abbreviations: moDCs, monocyte-derived dendritic cells; hpi, hours post-infection; IPA, ingenuity pathway analysis; ZIKV, Zika virus; MDM, monocyte-derived macrophage.

**A**



**B**

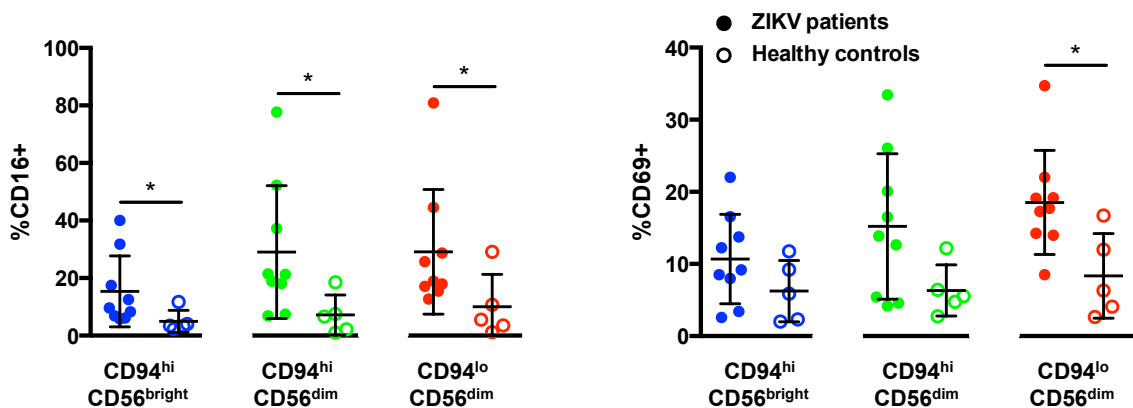
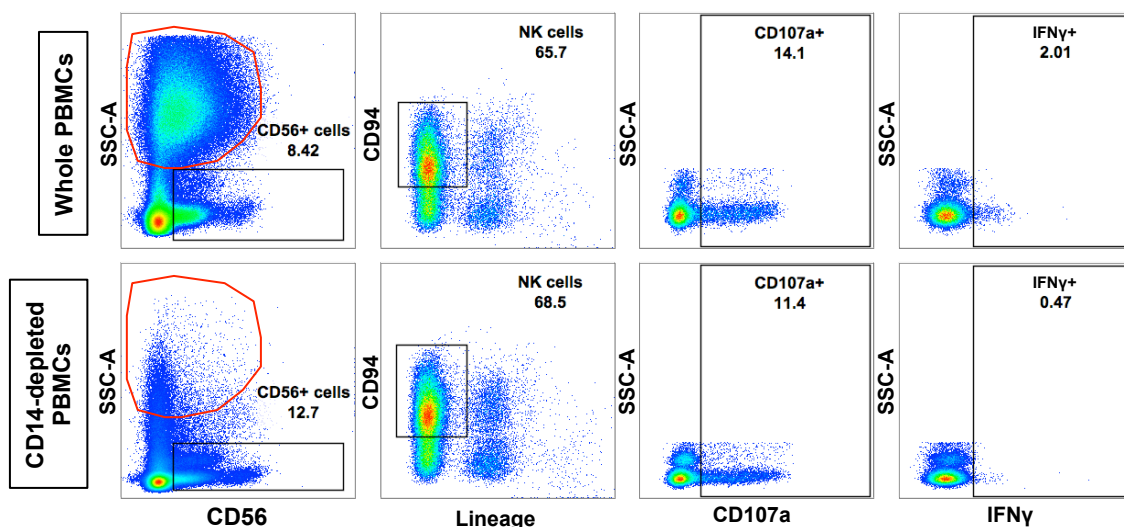
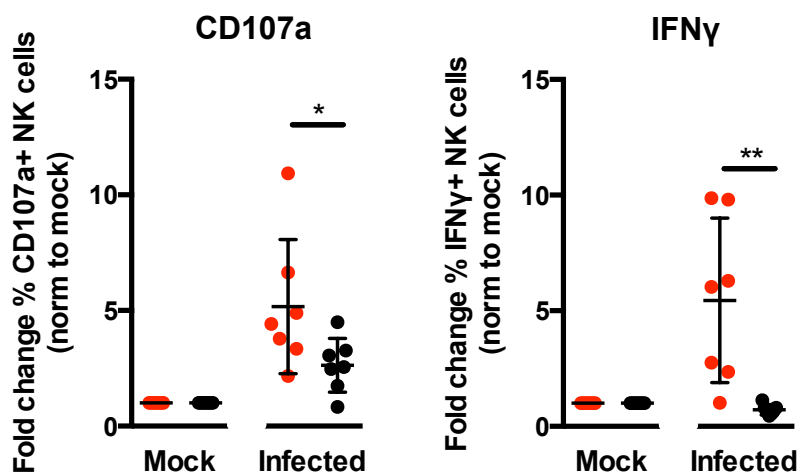


**Figure 5: Activation of CD56<sup>+</sup> cells in patients infected with ZIKV.** (A) Gating strategy of CD56<sup>+</sup> cell subsets and their expression of CD16 and CD69. CD56<sup>+</sup> cells were first gated from CD45<sup>+</sup> lymphocytes from peripheral blood mononuclear cells isolated from patients. These populations were further gated into three populations based on the expression of surface marker CD94: CD94<sup>hi</sup>CD56<sup>bright</sup> cells (blue), CD94<sup>hi</sup>CD56<sup>dim</sup> (green) and CD94<sup>lo</sup>CD56<sup>dim</sup> (red). The data presented correspond to a representative patient infected with ZIKV. Cells from a healthy control are overlaid and depicted as the black population (Q8). (B) Compiled data on the percentage of gated subsets that are positive for CD16 (Q5 and Q6) and CD69 (Q6 and Q7). Patients (n=9) are depicted as filled circles, and healthy controls (n=5) are depicted as clear circles. All data are presented as mean ± SD. \**P* < 0.05, by Mann Whitney *U* test, two tailed. Abbreviations: NK, natural killer; ZIKV, Zika virus.

**A**



**B**



● Whole PBMCs ● CD14-depleted PBMCs

**C**

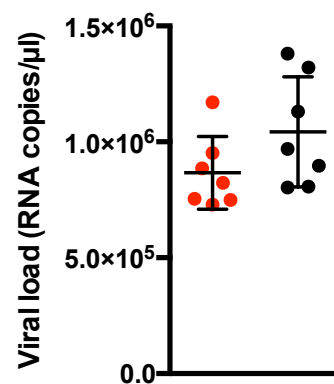


**Figure 6: Role of monocytes in NK-cell activity.** Full PBMCs and CD14-depleted PBMCs ( $2 \times 10^6$  cells per infection) were infected with Zika virus (ZIKV) at MOI 10 and harvested at 36 hpi. **(A)** Gating strategy of CD94<sup>+</sup>CD56<sup>+</sup>Lineage<sup>+</sup> NK cells and their expression of CD69, CD107a and IFN $\gamma$ . Plots from one representative donor are shown. The red circle indicates the presence or absence of CD14<sup>+</sup> monocytes. **(B)** Compiled percentages of CD107a and IFN $\gamma$ -positive NK cells (depicted in **(A)**) as normalized to the respective mock sample. **(C)** Viral load in the infected cells. Data shown were derived from seven donors. Lineage markers CD3, CD19, CD20 and CD14 have been included to rule out the presence of non-NK cells. All data are presented as mean  $\pm$  SD. \* $P < 0.05$ , \*\* $P < 0.01$ , by Mann Whitney  $U$  test, two tailed. Viral load data was not statistically significant between the two conditions by Mann Whitney  $U$  test, two tailed. Abbreviations; NK, natural killer; PMBC, peripheral blood mononuclear cell; hpi, hours post-infection.

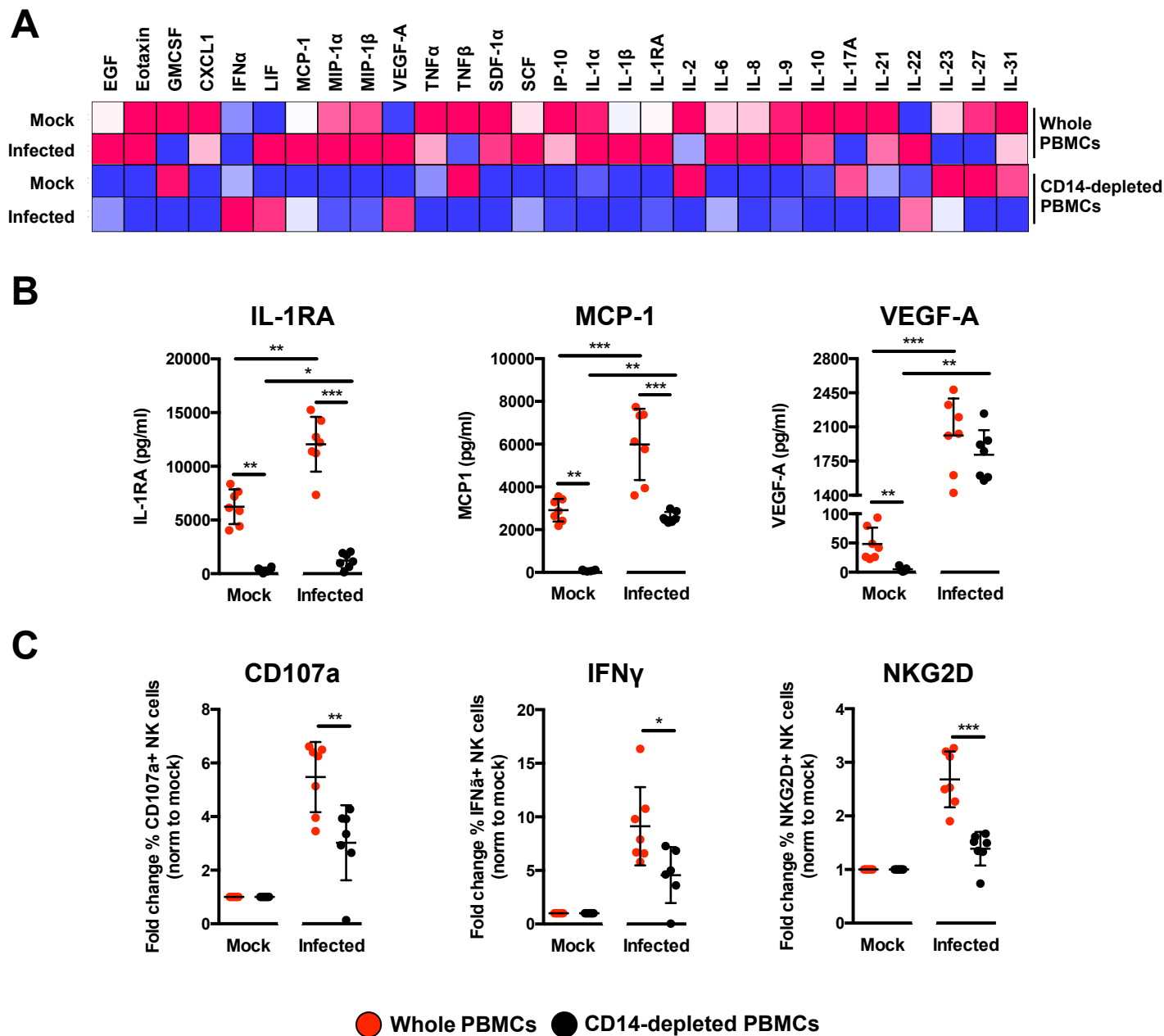


**Figure 7: Immune profiling of ZIKV-infected PBMCs.** (A) Immune mediators in the culture supernatant of ZIKV-infected PBMCs and CD14-depleted PBMCs were quantified with a 45-plex microbeads assay. Concentrations were scaled between 0 and 1. (B) Bar-charts of three cytokines, which levels were significantly affected by both the depletion of CD14<sup>+</sup> monocytes and ZIKV infection. (C) Stimulatory capacity of the culture supernatants were further evaluated with freshly isolated PBMCs. Culture supernatant was added in a ratio of 1:10 and cells were harvested at 36 hours post-stimulation. Compiled percentages of CD107a, IFN $\gamma$ , and NKG2D-positive CD94<sup>+</sup>CD56<sup>+</sup> NK cells are shown as normalized to the respective mock sample. Data displayed were derived from seven donors. Lineage markers CD3, CD19, CD20 and CD14 have been included to rule out the presence of non-NK cells. All data are presented as mean  $\pm$  SD. \* $P < 0.05$ , \*\* $P < 0.01$ , \*\*\* $P < 0.001$ , by Mann Whitney  $U$  test, two tailed. Abbreviations: NK, natural killer; PMBC, peripheral blood mononuclear cell.



**Table 1: Summary of nucleotide differences at specific genome positions**

Position in consensus sequence <sup>A</sup>	Nucleotide difference	Sample(s)	
1904	g → a	D1 MNC ZIKV 72hpi	
2673	t → c	D2 MDM ZIKV 24hpi	D2 MNC ZIKV 72hpi
2815	t	D1 MDM ZIKV 24hpi D2 MDM ZIKV 72hpi D2 MNC ZIKV 72hpi	D2 MDM ZIKV 24hpi D1 MNC ZIKV 72hpi
	c	D3 MDM ZIKV 24hpi D4 MDM ZIKV 24hpi D5 MDM ZIKV 72hpi	D3 MDM ZIKV 72hpi D5 MDM ZIKV 24hpi PF/ZIKV/HPF/2013
4211	a	D3 MDM ZIKV 24hpi D4 MDM ZIKV 24hpi D5 MDM ZIKV 72hpi	D3 MDM ZIKV 72hpi D5 MDM ZIKV 24hpi PF/ZIKV/HPF/2013
	g	D1 MDM ZIKV 24hpi D2 MDM ZIKV 72hpi D2 MNC ZIKV 72hpi	D2 MDM ZIKV 24hpi D1 MNC ZIKV 72hpi
10253	t → c	D1 MDM ZIKV 24hpi	D2 MNC ZIKV 72hpi
10472	t → c	D1 MNC ZIKV 72hpi	

The phylogenetic tree shown in Figure 3B revealed specific nucleotide differences at 6 different positions within the consensus sequence. All samples included had a mean coverage of greater than 10. PF/ZIKV/HPF/2013 represents the virus used for the infection and therefore, denoted as the reference sample in this analysis. Abbreviations: MNC, monocytes; MDM, monocyte-derived macrophage. <sup>A</sup>Note that minor variant file numbering of positions starts at 0 rather than 1.

**Table 2: Selected nucleotide positions from the minor variants file of the inoculum**

Position in consensus sequence <sup>A</sup>	Frequency of minor nucleotide variants				
	A	C	G	T(U)	D (A/G/T)
1904	0.11324	0	0.88601	0.00074	0
2673	0.00681	0.11779	0.000619	0.87476	0
2815	0.00876	0.64463	0	0.34659	0
4211	0.65122	0	0.34815	0.000626	0
10253	0.000891	0.11229	0	0.8868	0
10472	0.00108	0.00543	0.00108	0.99239	0

Table showing the frequency distribution of minor nucleotide variants at six positions in the consensus sequence. Major variant (i.e. the consensus nucleotide) at each position is indicated by the nucleotide with the highest frequency. <sup>A</sup>Note that minor variant file numbering of positions starts at 0 rather than 1.